New reference materials, analytical procedures, and data reduction strategies for Sr isotope measurements in geological materials by LA-MC-ICP-MS

Jacob Mulder[1,2], Graham Hagen-Peter[3,4], Teresa Ubide[1], Rasmus Andreasen[3], Ellen Kooijman[5], Melanie Schmitt[5], Yu-Xing Feng[1,6], Bence Paul[7,8], Andreas Karlsson[5], Christian Tegner[3], Charles Lesher[3,9], Fidel Costa[10]

[1]School of Earth and Environmental Sciences, The University of Queensland, Australia
[2]Department of Earth Sciences, University of Adelaide, Australia
[3]Department of Geoscience, Aarhus University, Denmark
[4]Geological Survey of Norway
[5]The Vegacenter, Swedish Museum of Natural History
[6]Southern Marine Science and Engineering Guangdong Laboratory (Zhuhai), Zhuhai, China
[6]Department of Earth Science, University of California, Santa Barbara
[7]School of Geography, Earth and Atmospheric Sciences, The University of Melbourne, Victoria, Australia
[8]Elemental Scientific Lasers, LLC. Bozeman, Montana, USA
[9]Department of Earth and Planetary Sciences, University of California, Davis, California, USA
[10]Institut de Physique du Globe de Paris, France

This is a non-peer reviewed paper uploaded to *EarthArXiv*
(submitted to *Geostandards and Geoanalytical Research*)

We welcome your feedback!

jack.mulder@adelaide.edu.au
t.ubide@uq.edu.au
@teresaubide (Twitter)

New reference materials, analytical procedures, and data reduction strategies for Sr isotope measurements in geological materials by LA-MC-ICP-MS

Jacob Mulder[1,2], Graham Hagen-Peter[3,4], Teresa Ubide[1], Rasmus Andreasen[3], Ellen Kooijman[5], Melanie Kielman-Schmitt[5], Yue-Xing Feng[6], Bence Paul[7,8], Andreas Karlsson[5], Christian Tegner[3], Charles Lesher[3,9], Fidel Costa[10]

[1]School of Earth and Environmental Sciences, The University of Queensland, Queensland, Australia

[2]Department of Earth Sciences, University of Adelaide, Adelaide, Australia

[3]Department of Geoscience, Aarhus University, Denmark

[4]Geological Survey of Norway

[5]The Vegacenter, Swedish Museum of Natural History, Sweden

[6]Southern Marine Science and Engineering Guangdong Laboratory (Zhuhai), Zhuhai, China

[7]School of Geography, Earth and Atmospheric Sciences, The University of Melbourne, Victoria, Australia

[8]Elemental Scientific Lasers, LLC. Bozeman, Montana, USA

[9]Department of Earth and Planetary Sciences, University of California, Davis, California, USA

[10]Institut de Physique du Globe de Paris, France

ABSTRACT

Laser ablation multi-collector mass spectrometry (LA-MC-ICP-MS) has emerged as the technique of choice for *in situ* measurements of Sr isotopes in geological minerals. However, the method poses analytical challenges and there is no widely adopted standardised approach to collecting these data or correcting the numerous potential isobaric inferences. Here, we outline practical analytical procedures and data reduction strategies to help establish a consistent framework for collecting and correcting Sr isotope measurements in geological materials by LA-MC-ICP-MS. We characterise a new set of plagioclase reference materials, which are available for distribution to the community, and present a new data reduction scheme for the *Iolite* software package to correct isobaric interferences for different materials and analytical conditions. Our tests show that a combination of Kr-baseline subtraction, Rb-peak-

stripping using βRb derived from a bracketing glass standard, and a CaCa/CaAr correction for plagioclase and CaCa/CaAr + REE^{2+} correction for rock glasses, yields the most accurate and precise $^{87}Sr/^{86}Sr$ measurements for these materials. Using the analytical and correction procedures outlined herein, spot analyses using a beam diameter of 100 μm or rastering with a 50—65 μm diameter beam can readily achieve <100 ppm 2SE internal precision for $^{87}Sr/^{86}Sr$ measurements for materials with <1000 ppm Sr.

INTRODUCTION

Long-lived radiogenic isotope systems, such as ^{87}Rb-^{87}Sr, ^{176}Lu-^{176}Hf, ^{147}Sm-^{143}Nd, and $^{238,235}U$-$^{206,207}Pb$, provide key insight into the interactions between magmatic reservoirs in Earth's crust and mantle. Although traditionally measured in bulk rock samples, these isotopic tracers can now be routinely analysed *in situ* with suitable precision to allow detailed records of open system magmatic processes and related volcanic behaviour and hydrothermal activity to be reconstructed from individual crystals (e.g., Chadwick et al., 2007; Davidson et al., 2007; Hepworth et al., 2020; Cho et al., 2022). The ^{87}Rb-^{87}Sr system is particularly well-suited to studying the spectrum of magmatic processes as radiogenic Sr (expressed as $^{87}Sr/^{86}Sr$) can be measured in a variety of Ca-bearing, rock-forming minerals including plagioclase, carbonates, and clinopyroxene, accessory phases such as apatite, and groundmass material. This versatility offers a distinct advantage over *in situ* measurements of other long-lived radiogenic isotope tracers, which are commonly limited to rare earth element (REE)- or Pb-rich accessory minerals that have a low modal abundance, are typically fine-grained, and may only precipitate in certain bulk rock compositions or during a narrow interval in the evolution of a magmatic system.

Prior to the early 2010's, most *in situ* radiogenic Sr isotope measurements were made by micro-milling followed by dissolution, chemical purification, and TIMS or solution-MC-ICP-MS (Fig. 1). These methods can yield high-precision data (<<100 ppm 2SE for $^{87}Sr/^{86}Sr$) but are time consuming and have a spatial resolution generally restricted to several hundred micrometres (Charlier et al., 2006). Consequently, the past decade has seen a dramatic uptake of laser ablation multi-collector inductively coupled plasma mass spectrometry (LA-MC-ICP-MS) for *in situ* measurements of radiogenic Sr isotopes (Fig. 1). Although solution-based analyses remain the technique of choice for high-precision Sr isotope measurements LA-MC-ICP-MS is a rapid and cost-effective method that can achieve the high spatial resolution

(≤150 μm) and precision needed to investigate many geological processes (e.g., Edwards et al., 2019 Hagen-Peter et al., 2019). However, there are numerous analytical challenges related to elemental and molecular interferences (Woodhead et al., 2005, Ramos et al., 2004, Vroon et al., 2008; Jochum et al., 2009; Kimura et al., 2013; Zhang et al., 2018) that have hampered Sr isotope measurements by laser ablation.

The development of ICP-MS instruments incorporating collision-reaction cells enables online chemical separation of the interferences inherent to *in situ* Sr isotope measurements (e.g., Zack and Hogmalm 2016; Bevan et al., 2021). "Triple-quadrupole" instruments (ICP-MS/MS)—with a quadrupole mass analyser on either side of a collision cell —are now relatively common but the optimal precision for $^{87}Sr/^{86}Sr$ measurements using these instruments is lower than that of LA-MC-ICP-MS. Bolea-Fernandez et al. (2016) demonstrate repeatability of ~560—1080 ppm (2 RSD) in $^{87}Sr/^{86}Sr$ for measurements of rock glass reference materials with Rb/Sr of ~0.02—0.67 using 20—85-micron-diameter laser spots. More recently, Rösel and Zack (2021) report uncertainties of ~9000—11000 ppm (2RSE, internal) for $^{87}Sr/^{86}Sr$ measurements from 50—60-micron single spot ablations of the reference glass BCR-2G with moderate Rb/Sr (~0.137). The online chemical separation of ^{87}Sr and ^{87}Rb by ICP-MS/MS is critical for accurate $^{87}Sr/^{86}Sr$ measurements in matrices with high Rb/Sr, but MC-ICP-MS yields superior precision in $^{87}Sr/^{86}Sr$ for low- to moderate Rb/Sr matrices (see below). More recently, Bevan et al. (2021) demonstrated the potential of using a multi-collector mass spectrometer with a collision cell (MC-ICP-MS/MS) to accurately measure Sr isotopes *in situ* and interference-free in high Rb/Sr matrices with a precision comparable to the traditional LA-MC-ICP-MS approach outlined in this study. Although the development of LA- MC-ICP-MS/MS for Sr isotope analysis shows future potential, commercially available MC-ICP-MS/MS instruments are not yet widespread, and may never overtake the prevalence of "traditional" MC-ICP-MS. Similarly, *in situ* Sr isotope analysis by secondary-ion mass spectrometry (Gillespie et al., 2021; Jeon and Whitehouse, 2021) is also limited by the availability of these instruments. Consequently, LA-MC-ICP-MS using a standard multi-collector mass spectrometer remains the most accessible method for high-resolution *in situ* Sr isotope analysis.

In this contribution, we outline practical analytical and data reduction strategies for *in situ* Sr isotope measurements of geological materials by LA-MC-ICP-MS. Although we concentrate

on the application of *in situ* Sr isotope analysis of minerals to study magmatic processes, the strategies outlined here are also have broader geological applications (e.g., isotopic fingerprinting of feldspar for provenance studies; Mulder et al., 2019), and may be applicable to the biological and ecological sciences (e.g., Sr isotope analysis of bio-apatite; Brennan et al., 2015), archaeology (glass; Van Ham-Meert et al., 2018), and aqueous geochemistry (carbonates; Woodhead et al., 2005). Here we focus on plagioclase and groundmass as examples of common geological materials that are amenable to *in situ* Sr isotope analysis and pose distinct analytical challenges. The importance of potential inferences on Sr isotopes are first reviewed and then systematically evaluated by analysing a set of newly characterised plagioclase reference materials, which are available to the community, and previously characterised rock glass reference materials. Because the magnitudes of interferences on Sr isotope masses will inevitably differ among laboratories and between sample matrices, we provide a "data reduction scheme" for the *Iolite* software package (Paton et al., 2011) that can perform various combinations of corrections as required for different materials and analytical protocols. Finally, we show how our analytical procedures and data reduction strategies can be used to investigate magmatic processes at high-spatial resolution through a case study on the centennial 2010 explosive eruption at Merapi Volcano, Indonesia. We explore Sr-isotope variations in volcanic groundmass and plagioclase crystals containing complex internal textures and chemical zoning.

EXISTING PROTOCOLS TO CORRECT AND REPORT *IN* SITU SR ISOTOPE MEASUREMENTS

Accurately measuring any isotopic system by LA-MC-ICP-MS relies on the correction of fractionation of isotopes during ablation, ionisation, and transport (instrumental mass bias) and the removal of elemental and molecular species with the same approximate mass/charge ratio as the isotopic masses of interest (isobaric interferences). The efficacy of these corrections can be assessed by analysing matrix-matched reference materials of known isotopic composition or monitoring stable isotope ratios of the same element as the target isotope. Figure 2 summarises current literature standards on the analysis and reporting of LA-MC-ICP-MS Sr isotope studies of plagioclase published over the past three decades (n = 65). It is apparent from Figure 2 that there is no single widely adopted protocol for measuring,

correcting, or reporting Sr isotope data from plagioclase, which is the most common magmatic mineral targeted for *in situ* Sr isotope analysis. The proportion of studies that report Sr isotope data from matrix-matched secondary reference materials is notably low (only 19% of studies). Instead, many studies have employed carbonate (~25 % of studies) or rock glasses (24% of studies) as secondary reference materials to assess the accuracy of instrumental mass bias and interference corrections. This likely reflects the availability of carbonate reference materials in the form of modern shells or coral, which generally have the homogenous Sr isotopic composition of modern seawater, and the wide distribution of rock glass reference materials that are also employed for other laser ablation analyses. In contrast, well-characterised plagioclase reference materials are scarce.

Few studies report stable isotope ratios $^{84}Sr/^{86}Sr$ and $^{84}Sr/^{88}Sr$ (only 21% of studies), which may be due to these ratios being significantly affected by isobaric interferences that otherwise do not impact—or impact to a lesser degree—the radiogenic Sr isotope ratio ($^{87}Sr/^{86}Sr$, see below). In summary, there is no consensus on the magnitude of the numerous different isobaric interferences inherent to *in situ* Sr isotope measurements by LA-MC-ICP-MS (e.g., Woodhead et al., 2005; Ramos et al., 2004) and they are often assumed to be negligible without being directly monitored or quantified (Fig. 2).

ANALYTICAL CHALLENGES OF *IN SITU* SR ISOTOPE MEASUREMENTS

In the absence of any isobaric interferences, accurate determination of $^{87}Sr/^{86}Sr$ would require the measurement of only three isotopes: ^{87}Sr, ^{86}Sr, and another non-radiogenic isotope (typically ^{88}Sr) to calculate instrumental mass bias. However, there are multiple isobaric interferences on all Sr isotopes during LA-MC-ICP-MS analysis (Fig. 3) and correcting these interferences is critical to the method. We will not detail all isobaric interferences that could theoretically be encountered during *in situ* Sr isotope measurements, some of which have already been systematically studied and reviewed elsewhere (e.g., Woodhead et al., 2005; Ramos et al., 2004; Vroon *et al*., 2008; Kimura *et al., 2013*; Müller and Anczkiewicz, 2016; Tong et al., 2016). Instead, we focus on what are likely the most common and significant isobaric interferences in geological materials and outline correction strategies.

Kr interferences: Krypton is a noble gas that is present in varying concentrations in the ICP and carrier gases (Ar and He) used for LA-MC-ICP-MS analysis (Woodhead et al., 2005). Small concentrations of Kr may also be present in sample materials (Kimura *et al*., 2013). Isotopes of Kr interfere on ^{86}Sr, which is used to calculate instrumental mass bias and the radiogenic $^{87}Sr/^{86}Sr$ ratio, and on ^{84}Sr, which is used in stable isotope ratios ($^{84}Sr/^{86}Sr$ and $^{84}Sr/^{88}Sr$). Figure 4A shows a simulation of the error in $^{87}Sr/^{86}Sr$ if Kr is not subtracted from the Sr signals. This is the single largest potential source of error in *in situ* Sr isotope measurements by LA-MC-ICP-MS.

Kr interferences can be corrected by subtracting the pre-ablation on-peak signal on masses 86 and 84 from the signal during ablation (baseline subtraction) or by "peak-stripping". Baseline subtraction is the most widely adopted approach to correcting Kr interferences and assumes that the Kr contribution to the 86 and 84 signals does not change during analysis, although Kimura *et al*. (2013) show that Kr signals can be affected by plasma loading during ablation. Peak-stripping relies on a relatively small Kr signal on mass 82 or 83 to calculate ^{84}Kr and ^{86}Kr using canonical Kr isotope ratios and assumes the raw signal on mass 82 or 83 is due to Kr alone.

An alternative approach to correcting Kr interferences is outlined by Kimura *et al*. (2013) who observed a negative linear correlation between measured (baseline-subtracted, ^{87}Rb-peak stripped, and mass-bias-corrected) $^{87}Sr/^{86}Sr$ and $^{84}Sr/^{86}Sr$ across several analytical sessions. They used this correlation to empirically derive a correction factor based on the measured $^{87}Sr/^{86}Sr$ and $^{84}Sr/^{86}Sr$ and successfully applied it to reproduce the $^{87}Sr/^{86}Sr$ of several plagioclase samples confirmed by micro-milling and thermal ionisation mass spectrometry (TIMS). This approach will only be robust if a correlation between measured $^{87}Sr/^{86}Sr$ and $^{84}Sr/^{86}Sr$ is observed, requiring at least one homogeneous reference material.

Konter & Storm (2014) developed a routine for an online correction of Kr interferences on Sr masses by solving linear or series-expanded exponential mass bias laws to determine the magnitude of Kr interferences needed to explain the offsets between the measured and reference $^{84}Sr/^{88}Sr$ and $^{86}Sr/^{88}Sr$. This approach has the advantage of not relying on a relatively small ^{83}Kr signal for the correction, which propagates error into the final $^{87}Sr/^{86}Sr$ ratio. This routine was developed specifically for MC-ICP-MS measurements of purified Sr solutions, in

199 which interferences on ^{84}Sr and ^{86}Sr from species other than Kr are likely very minor. It may
200 not be effective if there are additional interferences on ^{84}Sr and ^{86}Sr other than Kr and is not
201 considered further in this study. Instead, our new data reduction scheme adopts the baseline
202 subtraction approach as it is easily employed in analytical routines and appears to be generally
203 effective for correcting $^{87}Sr/^{86}Sr$.
204
205 **Molecular interferences:** All materials routinely targeted for LA-MC-ICP-MS Sr isotope
206 measurements are calcium-rich. Isotopologues of Ca dimers (CaCa) and calcium argides
207 (CaAr) interfere on all isotopes of Sr (Fig. 4B). Although intuitively these molecules may be
208 expected to be major interferences during the analysis of Ca-bearing minerals, only ~3% of
209 these Ca-bearing isotopologues have masses in the range of interest for Sr isotope
210 measurements (masses 82–88), which reduces their impact on Sr isotope ratios (Fig. 3B and
211 3C). Additional molecular interferences that have been considered during the analysis of
212 plagioclase include NaNi (with Ni likely derived from mass spectrometer cones) and
213 CaAlO/ArAlO, which interfere on all Sr isotope masses (Kimura *et al*. 2013). Figure 4B
214 shows a simulation of the error in $^{87}Sr/^{86}Sr$ introduced by unsubtracted signals from
215 CaCa/CaAr, NaNi and CaAlO/ArAlO molecular interferences. The magnitudes of these
216 errors are relatively small (< 50 ppm) for the signals on mass 82 and 83 observed during the
217 analysis of plagioclase in this study. CaPO molecules may also present a significant
218 interference on mass 87 (and 88 to a lesser extent) in phosphorus-rich materials, such as
219 apatite (Horstwood et al. 2008; Wilmes et al., 2018; Griffin et al., 2021). A preliminary
220 correction procedure for CaPO is included in the new Iolite data reduction scheme and will
221 be further developed and described in detail elsewhere (Supplementary files 3 and 4).
222
223 Interferences from CaCa/CaAr, NaNi, and CaAlO/ArAlO can be corrected by peak-stripping
224 after baseline subtraction of Kr (with or without prior REE^{2+} peak-stripping; see below).
225 Interference-free CaCa or CaAr can be monitored on mass 82 or 83 and canonical CaCa/CaAr
226 isotopologue ratios used to strip interferences from mass 83 (if mass 82 is used as the monitor)
227 and the four Sr masses. However, it is difficult to determine the relative contributions of CaCa
228 versus CaAr molecules to the interferences since the isotopic proportions of both molecules
229 are similar on masses 88 and 84. The CaCa and CaAr molecules also theoretically yield similar
230 M83/M82 precluding the use of this ratio to discern their contributions. Therefore, the accuracy

231 of $^{87}Sr/^{86}Sr$ ratios following CaCa/CaAr peak-stripping should be relatively insensitive to the
232 actual proportion of CaCa to CaAr molecules (Fig. 4B, Woodhead et al., 2005).
233
234 After correcting CaCa/CaAr interferences, the residual signal on mass 83 can be used to peak
235 strip NaNi and CaAlO/ArAlO from masses 84–88. The ratio of the signal on masses 83 and 82
236 can potentially be used to determine the importance of NaNi and CaAlO/ArAlO corrections as
237 baseline-subtracted signals from $^{40}(Ca/Ar)^{43}Ca$ and $^{40}(Ca/Ar)^{42}Ca$ alone should produce an
238 83/82 ratio of ~0.21. Because NaNi or CaAlO do not contribute to mass 82, significant
239 interferences from these molecules will lead to a higher 83/82 ratio.
240
241 **Rb interference:** Uncorrected ^{87}Rb signals are a potentially large source of error in $^{87}Sr/^{86}Sr$,
242 even for low-Rb materials like plagioclase (Fig. 4C). The ^{87}Rb interference can be corrected
243 using the signal of ^{85}Rb and the canonical $^{87}Rb/^{85}Rb$ ratio. However, because there are not two
244 interference-free Rb isotopes, instrumental mass bias of Rb cannot be internally calculated
245 during a measurement. The most common approach is to assume that the instrumental mass
246 bias factor for Rb (βRb) is equivalent to that of Sr (βSr). However, several studies adopting
247 this approach report large errors in $^{87}Sr/^{86}Sr$ for materials with high Rb/Sr, which can potentially
248 be explained by unconstrained differences between Rb and Sr mass bias (Davidson *et al*., 2001;
249 Ramos *et al*., 2004; Jackson & Hart, 2006). Jackson and Hart (2006) outlined an approach for
250 estimating the in-run βRb by using bracketing standards with known $^{87}Sr/^{86}Sr$ and solving the
251 following equation for βRb:
252
253 $$^{87}Sr/^{86}Sr_{ref} = [\ ^{87}(Sr,Rb) - ^{85}Rb * (^{87}Rb/^{85}Rb_{ref}) * (mass^{87}Rb/mass^{85}Rb)^{\beta Rb}] *$$
254 $$(mass^{87}Sr/mass^{86}Sr)^{\beta Sr} * (1/^{86}Sr_{cor})$$
255
256 *where:*
257 $^{87}Sr/^{86}Sr_{ref}$ *is the Sr isotope ratio of the bracketing standard*
258 $^{87}(Sr,Rb)$ *is the signal on mass 87 with all other interferences subtracted*
259 ^{85}Rb *is the raw signal on mass 85*
260 $^{87}Rb/^{85}Rb$ *is a canonical natural Rb isotope ratio*
261 $^{86}Sr_{cor}$ *is the interference-corrected* ^{86}Sr *signal*
262

Due to the very low Rb/Sr of the minerals commonly targeted for Sr isotope analysis (e.g., plagioclase, carbonate, apatite), glass reference materials with moderate Rb/Sr ratios, such as BCR-2G ($^{87}Rb/^{86}Sr$ ~0.388, elemental Rb/Sr = 0.137), can be used as bracketing standards to estimate βRb (Jackson & Hart, 2006). Figure 4D shows a simulation of the error in $^{87}Sr/^{86}Sr$ resulting from differences between βRb and βSr illustrating potential errors up to 10^3 ppm even for materials with moderate Rb/Sr.

Elemental Rb/Sr used for age-correction: Uncorrected elemental fractionation of Rb and Sr during analysis will cause errors in age-corrected $^{87}Sr/^{86}Sr$ ratios, which rely on accurate $^{87}Rb/^{86}Sr$ measurements of samples (Fig. 4C, inset). Like the βRb-βSr offset outlined above, elemental fractionation can be corrected with sample-standard bracketing using a glass reference material with moderate Rb/Sr. This approach, however, assumes that the magnitude of Rb-Sr fractionation observed in the glass reference material is identical to that in the samples. Nevertheless, errors arising from poorly constrained Rb/Sr fractionation are likely to be negligible for the minerals commonly analysed for radiogenic Sr isotopes, as their typically low Rb/Sr does not lead to a significant age-correction, even for relatively old samples (Fig. 4C, inset). This correction is more important for old samples with high Rb/Sr.

Doubly charged interferences: Doubly charged ions of elements with atomic masses of 160–180 have effective mass/charge (m/z) ratios of 80–90 and can interfere on Sr isotope masses. Isotopes of Er^{2+} and Yb^{2+} are the most important of the doubly charged interferences for Sr isotope measurements as they appear directly on all Sr isotope masses: ^{84}Sr ($^{168}Er^{2+}$, $^{168}Yb^{2+}$), ^{86}Sr ($^{172}Yb^{2+}$), ^{87}Sr ($^{174}Yb^{2+}$), and ^{88}Sr ($^{176}Yb^{2+}$), as well as on masses 83 ($^{166}Er^{2+}$) and 85 ($^{170}Er^{2+}$, $^{170}Yb^{2+}$), which are used to peak-strip interferences from CaCa/CaAr and Rb, respectively. Under typical analytical conditions (Supplementary File 1), the yield of doubly charged Er^{2+} and Yb^{2+} is low, with estimates ranging from 0.4% to 1.7% of total Er or Yb ions (e.g., Ramos et al., 2004; Kimura et al., 2013; Müller and Anczkiewicz, 2016). Together with Er and Yb, other elements capable of producing doubly charged species such as $^{164}Dy^{2+}$ on mass 82 (used for the CaCa/CaAr peak-stripping), $^{176}Hf^{2+}$and $^{176}Lu^{2+}$ (appearing at mass 88), may be present as minor substitutions in minerals or be sourced from inadvertently ablated REE-rich inclusions such as zircon, xenotime, or apatite. The magnitude of error in $^{87}Sr/^{86}Sr$ due to interferences from doubly charged ions of Er, Yb, and Lu are simulated in Figure 4E and can be significant (> 1000 ppm) for materials with elevated REE contents. Figure 5A shows the Er + Yb contents

and chondrite-normalised REE patterns for geological materials commonly analysed for Sr isotopes alongside typical ablation signals (Fig. 5B) and the error in $^{87}Sr/^{86}Sr$ due to uncorrected doubly charged interferences (Fig. 5C). Although not exhaustive, the analysis presented in Figure 5 suggests that signals from doubly charged Er and/or Yb are resolvable for materials with >5 ppm Er + Yb (e.g., BCR-2G) and translate to significant error in $^{87}Sr/^{86}Sr$ for materials with Er + Yb contents on the order of 10 ppm, as demonstrated by the two apatite reference materials.

The mass separation in the moderate mass/charge range of Sr isotopes enables monitoring of Er^{2+} and Yb^{2+} on "half-masses" in typical Faraday cup arrays. The contributions of $^{167}Er^{2+}$ (m/z = 83.5) can be measured on a detector situated between masses 83 and 84 and the contribution from $^{173}Yb^{2+}$ (m/z = 86.5) can be measured on a detector between 86 and 87. Because all significant interfering Er^{2+} and Yb^{2+} isotopes are non-radiogenic, they can be stripped using canonical isotope ratios. Our new *Iolite* data reduction scheme also uses the signal on mass 87.5 ($^{175}Lu^{2+}$) to peak-strip $^{176}Lu^{2+}$ from ^{88}Sr.

NEW PLAGIOCLASE REFERENCE MATERIALS

Plagioclase is the most common magmatic rock-forming mineral targeted for *in situ* Sr isotope analysis (Fig. 1). However, there are few widely available matrix-matched reference materials, which continues to hinder interlaboratory comparisons of data quality (Fig. 2). Xu et al. (2022) recently characterised a plagioclase reference material (BDL-suite plagioclase) with high Sr concentration, low Rb/Sr, low HREE, and homogeneous $^{87}Sr/^{86}Sr$. However, to our knowledge, there are few other widely used plagioclase community reference materials. We characterised a new set of plagioclase reference materials with a wide range of Sr concentration, which are described below and are available for distribution to the community (Table 1). The anorthite contents of the plagioclase reference materials were calculated from semi-quantitative micro-X-ray fluorescence (micro-XRF) at Aarhus University, Denmark, or scanning electron microscope energy-dispersive spectroscopy (SEM-EDS) at the Swedish Museum of Natural History. Nominal Sr concentration ranges were determined by isotope-dilution TIMS analyses at the Swedish Museum of Natural History and from LA-MC-ICP-MS at Aarhus University by comparing ^{88}Sr signals to a rock glass standard (BCR-2G) with known Sr concentration. These Sr concentrations are considered approximate in the absence of a matrix-matched standard and without normalization to an internal elemental standard.

The range of Rb/Sr in each plagioclase reference material was determined by normalization of LA-MC-ICP-MS signals to Rb/Sr = 0.137 for BCR-2G to account for Rb-Sr elemental fractionation during the measurements. More details of the analytical protocols follow the descriptions of the reference plagioclase.

AMNH-107160 Labradorite: AMNH-107160 is an optically clear labradorite crystal from Casas Grandes, Chihuahua, Mexico. We acquired a ~5.5 g cut from a ~16 g crystal at the American Museum of Natural History. It was originally described as bytownite, but micro-XRF analyses on several fragments yielded ~54% An (molar percent anorthite), classifying as labradorite. Strontium concentrations from ID-TIMS of two fragments were ~690 and 990 ppm. Strontium concentrations from LA-MC-ICP-MS measurements range from 551 to 877 ppm, with a median value of 673 ppm (Supplementary File 5). The $^{87}Rb/^{86}Sr$ measured in 105 LA-MC-ICP-MS analyses is relatively uniform from 0.0009–0.0016, with a median value of 0.0010 and 2 SD of 0.00021 (Supplementary File 5). TIMS measurements were made on two fragments at the Swedish Natural History Museum. Solution MC-ICP-MS measurements were performed on nine fragments at Aarhus University. LA-MC-ICP-MS measurements were done on at least fifteen different fragments at Aarhus University and The University of Queensland.

G29958 Anorthite: G29958 comprises well-developed white translucent anorthite crystals, which occur in cavities within basalt from Mt Vesuvius, Italy. Individual crystals are mostly 5–6 mm. SEM-EDS analyses yielded ~90 % An. Strontium concentration from ID-TIMS of one fragment was ~2800 ppm. Strontium concentrations from LA-MC-ICP-MS measurements are highly variable, ranging from 1235 to 3229 ppm, with a median value of 1611 ppm. The $^{87}Rb/^{86}Sr$ from 64 analyses ranges from 0.00007 to 0.00024, with a median value of 0.00013 and 2 SD of 0.0001 (excluding one significantly higher value of 0.0012). TIMS measurement was made on one crystal fragment at the Swedish Natural History Museum and solution MC-ICP-MS measurements were made on seven fragments at Aarhus University. LA-MC-ICP-MS measurements were done on at least 25 different fragments at Aarhus University and the University of Queensland.

Hrappsey 14-2 Bytownite: Hrappsey 14-2 comprises pale green translucent bytownite crystals from an anorthosite xenolith contained in basalt from Hrappsey Island, Iceland (Kristmannsdottir, 1997). Individual crystals range from 1 to several mm in size. Micro-XRF

analyses yielded ~77 % An. Strontium concentrations from LA-MC-ICP-MS measurements vary from 222 to 270 ppm, with a median value of 243 ppm. The $^{87}Rb/^{86}Sr$ from 46 analyses ranges from 0.0008 to 0.0946, with a median value of 0.0023 and 2 SD of 0.0391. Solution MC-ICP-MS measurements were done on 8 individual crystals at Aarhus University. LA-MC-ICP-MS measurements were done on 11 individual crystals at Aarhus University and 3 crystals at the University of Queensland

ANALYTICAL METHODS

Solution MC-ICP-MS and TIMS measurements

Strontium isotopes of several fragments (4–9) of each of the reference plagioclases were determined following digestion and chemical purification of Sr by standard ion-chromatography protocols at Aarhus University in three different batches. Purified Sr solutions were measured by MC-ICP-MS (Nu Plasma II) coupled to a desolvating nebulizer. All results are reported in Supplementary File 2. Samples were concentration-matched with solutions of NBS 987 measured every 2–3 samples throughout the session. All measurements were corrected for Kr and Rb interferences, mass-bias corrected using an exponential law and $^{88}Sr/^{86}Sr = 8.375209$ and normalised to $^{87}Sr/^{86}Sr = 0.710248$ for NBS 987 (Weiss et al., 2006). A combination of at least two fractions of the rock glass reference material BHVO-2G, BCR-2G, and BIR1-G were included in each batch from sample digestion, Sr purification, and, finally, measurement. Triplicate measurements of four fractions of BHVO-2G measured throughout each session yielded an average $^{87}Sr/^{86}Sr = 0.703492 \pm 0.000039$ (2 SD), in agreement with the reference value of $^{87}Sr/^{86}Sr = 0.703487$ (Weiss *et al.*, 2006). Triplicate measurements of an aliquot of BIR1-G measured in one session yielded $^{87}Sr/^{86}Sr = 0.703097 \pm 0.000010$ (2 SD), in agreement with a reference value of $^{87}Sr/^{86}Sr = 0.703108$ (Pin *et al.*, 1994; re-normalised to $^{87}Sr/^{86}Sr = 0.710248$ for NBS 987). Aliquots of BCR-2G measured in the second and third sessions yielded $^{87}Sr/^{86}Sr = 0.705008 \pm 0.000017$ and $^{87}Sr/^{86}Sr = 0.705012 \pm \pm 0.000017$, respectively, in agreement with a reference value of $^{87}Sr/^{86}Sr = 0.705019$ (Weiss et al., 2006). An aliquot measured in the first session yielded a significantly higher $^{87}Sr/^{86}Sr = 0.705358$. The source of the inaccuracy is unknown, but we emphasize that BHVO-2G measured in the same session, and all other standard aliquots throughout other sessions, were reproduced accurately. TIMS measurements were carried out on two fragments of AMNH-107160 and one fragment of G29958 at the Swedish Natural History Museum. Following dissolution of the fragments, an ^{84}Sr-enriched spike was added to one aliquot of the solution to

395 determine Sr concentrations, while another aliquot was left unspiked. Following purification
396 of Sr by standard ion-chromatography protocols, samples were loaded onto Re filaments with
397 a Ta activator, and isotope measurements were carried out on a Thermo Scientific TRITON
398 TIMS. Measurements were mass-bias corrected using an exponential law and $^{88}Sr/^{86}Sr$ =
399 8.375209 and normalised to $^{87}Sr/^{86}Sr$ = 0.710248 for NBS 987. The isotopic measurements of
400 the unspiked aliquots are reported in Supplementary File 2.
401
402 **LA-MC-ICP-MS measurements and data reduction**
403 Strontium isotopes in the reference plagioclase were measured by LA-MC-ICP-MS at Aarhus
404 University and The University of Queensland to evaluate homogeneity, data accuracy, and
405 reproducibility. The method employed at Aarhus University is outlined in Hagen-Peter et al.
406 (2019) and the instrumental set-up and analytical conditions are described in Supplementary
407 File 1. The method at The University of Queensland differs slightly from that at Aarhus
408 University and is described further below. The analytical set up at The University of
409 Queensland comprises an ASI RESOlution 193 nm excimer laser ablation system and a Lauren
410 Technic S155 double volume ablation cell coupled to a Nu Instruments Nu Plasma II MC-ICP-
411 MS (Supplementary File 1). Prior to the analytical session, the mass spectrometer is tuned
412 during ablation of a modern mollusc shell containing ~ 3000 ppm Sr to refine the peak shape
413 of Sr isotope masses and achieve a signal of at least 4-5V on mass 88 to optimise sensitivity.
414 A second stage of tuning is performed during ablation of NIST610 and aimed to minimise
415 oxide formation by reducing Th/ThO^+ to <1%, and to supress the formation of doubly charged
416 REE ions (monitored on half-masses). Following tuning, ablation of the plagioclase reference
417 materials was performed using a 50 to 100 μm spot size, fluence of 4 Jcm^{-2}, and 10 Hz repetition
418 rate. Each analysis involved 40 seconds of baseline measurement, 45 seconds of ablation, and
419 12 seconds washout between analyses. We also performed 200-μm-long raster analyses with a
420 scan speed of 2 μm/s, using the same laser conditions. The ablated aerosol was transported to
421 the torch in a mixture of He (300—310 ml/min), Ar (965 ml/min), and N_2 (1.2 ml/min) gas.
422 The mass spectrometer was operated at an RF power of 1300 W and ion beams with
423 mass/charge ratios of 82—88, including half masses at 82.5—87.5, measured in statistic mode
424 on Faraday cups over 0.1 second integration intervals.
425
426 All corrections were performed using our custom data reduction scheme developed for *Iolite 4*
427 (Supplementary files 3 and 4). In brief, the new data reduction scheme includes baseline

correction using a smoothed cubic spline, calculation of βRb and Rb-Sr fractionation factors from repeat analyses of BCR-2G, correction for ^{87}Rb interference, and correction for other isobaric interferences as necessary (see details below). The accuracy of the LA-MC-ICP-MS analyses of our new plagioclase reference materials was assessed by comparison to the solution values and by analysing the low Rb/Sr reference glasses BIR1-G and BHVO-2G as secondary standards.

RESULTS AND DISCUSSION

Sr isotope homogeneity of plagioclase reference materials

Solution MC-ICP-MS and TIMS Sr isotope results for the reference plagioclase are provided in Supplementary File 2 and summarised in Table 1 and Figure 6. Solution analyses of 9 fragments (including triplicate measurements of 2 fragments) of AMNH-107160 yielded an average $^{87}Sr/^{86}Sr = 0.704371 \pm 0.000024$ (2 SD), in agreement with a TIMS value of 0.704365 ± 0.000015 (average for 2 fragments where the uncertainty is based on repeated measurement of NBS 987). Solution analyses of 7 fragments (including triplicate measurements of 3 fragments) of G29958 yielded an average $^{87}Sr/^{86}Sr = 0.707551 \pm 0.000022$ (2 SD), in agreement with the TIMS value of 0.707547 ± 0.000015 from one fragment. Solution analyses of 8 fragments (including quadruplicate measurements of each fragment) of Hrappsey 14-2 yielded an average $^{87}Sr/^{86}Sr = 0.703168 \pm 0.000018$ (2 SD). A compilation of 105 LA-MC-ICP-MS measurements of AMNH-107160 from six different sessions at Aarhus University and the Swedish Museum of Natural History yielded an average non-normalised $^{87}Sr/^{86}Sr$ of 0.704377 ± 0.000101 (2 SD; normalised to G29958; Supplementary File 5). A total of 65 measurements of G29958 from the same sessions yielded an average $^{87}Sr/^{86}Sr$ of 0.707549 ± 0.000058 (2 SD; normalised to AMNH-107160). A compilation of 46 measurements of Hrappsey 14-2 from one of the sessions yielded an average $^{87}Sr/^{86}Sr$ of 0.703198 ± 0.000126 (2 SD; normalised to AMNH-107160). These values represent biases of < ~45 ppm from solution MC-ICP-MS reference values and reproducibility of ~82–180 ppm (2 RSD) for plagioclase with a wide range of Sr concentration (total measured Sr signals from ~2.3–33.0 V in these sessions).

Based on our LA-MC-ICP-MS results, AMNH-107160, G29958, and Hrappsey 14-2 are homogeneous for Sr isotope ratios based on the low variability in the solution- and LA-MC-ICP-MS analyses of multiple fragments and the good agreement with TIMS values. Due to the greater number of fragments analyzed by solution MC-ICP-MS, and the absence of any

apparent systematic biases from the TIMS values, we take the averages of the solution data as the reference values for the plagioclase reference materials. We use AMNH-107160 as the primary reference material for normalising $^{87}Sr/^{86}Sr$ measurements made by LA-MC-ICP-MS because of the greater number of fragments of this crystal characterised by solution ICPMS. However, using G29958 as the primary reference material yields comparably accurate results.

Assessment of isobaric interferences on Sr isotope measurements by LA-MC-ICP-MS

The key strength of *in situ* Sr isotope analysis via LA-MC-ICP-MS is the wide range of materials that are amenable to the technique. However, this diversity of analytes requires a wide range of potential isobaric interferences to be considered (Fig. 3). These isobaric interferences are the most important source of error for *in situ* Sr isotope measurements (Fig. 4). The peak-stripping method for correcting isobaric interferences relies on typically low-intensity signals from non-Sr isotope masses or half-masses (Figs. 4 and 5), which can decrease the precision of the final radiogenic Sr isotope ratios, or even introduce additional bias. Therefore, evaluating which isobaric interference corrections are likely to be important for a given material is needed to obtain accurate radiogenic Sr isotope measurements without unnecessarily compromising precision.

Interferences from ^{86}Kr and ^{87}Rb account for the largest biases in $^{87}Sr/^{86}Sr$ (Fig. 4A and 4C) and will be inherent to LA-MC-ICP-MS Sr isotope measurements of most geological materials. Although alternative approaches for correcting Kr interferences may be equally as effective (e.g., Kimura et al., 2013; Konter & Storm, 2014), our *Iolite* data reduction scheme adopts an on-peak baseline subtraction for Kr correction as this approach is easy to employ in analytical routines and appears to be widely effective, at least for correcting $^{87}Sr/^{86}Sr$ measurements (but see below for further discussion of ^{84}Kr interference on ^{84}Sr). Similarly, because ^{87}Rb is a common and major interference on $^{87}Sr/^{86}Sr$, even in low Rb/Sr materials (Fig. 4C), ^{87}Rb interference correction should be an integral part of Sr isotope data reduction procedures. The importance of calculating the offset between βRb and βSr for the ^{87}Rb interference correction is summarised in Figure 7 for a series of glass reference materials with varying Rb/Sr. Figure 7A shows the residual error in $^{87}Sr/^{86}Sr$ assuming no offset between βRb and βSr whereas Figure 7B shows the residual error after calculating a βRb-βSr offset by calibration to BCR-2G. The results shown on Figure 7A suggest that $^{87}Sr/^{86}Sr$ measurements are generally inaccurate for all reference glasses if βRb=βSr with the magnitude of the residual error in

$^{87}Sr/^{86}Sr$ increasing with increasing Rb/Sr of the analyte. In contrast, calculating a βRb-βSr offset produces accurate $^{87}Sr/^{86}Sr$ measurements for reference glasses with Rb/Sr up to ~0.3 (i.e., the T1-G reference glass). These results demonstrate that calculating a βRb-βSr offset significantly improves the efficacy of ^{87}Rb interference corrections. Calculating this offset by standard-sample bracketing with a reference material with moderate Rb/Sr, such as the widely available BCR-2G reference glass, is easily accommodated into standard analytical routines. However, even after determining a βRb-βSr offset, our results suggest that accurate $^{87}Sr/^{86}Sr$ measurements via LA-MC-ICP-MS are limited to materials with low- to moderate Rb/Sr (< 0.30), in agreement with previous studies (Ramos et al., 2004; Vroon et al., 2008).

In addition to performing Kr and Rb interference corrections, the new *Iolite* data reduction scheme (Supplementary files 3 and 4) allows users to quickly and systematically evaluate which combination of additional isobaric interference corrections are most appropriate for their measurements. This approach is illustrated in Figure 8A and 8B, which summarise the accuracy and precision of $^{87}Sr/^{86}Sr$ measurements of plagioclase and mafic to intermediate rock glass reference materials (as a proxy for basaltic to andesitic groundmass), respectively, subject to various combinations of isobaric interference corrections. For example, the leftmost sets of analyses in each panel of Figure 8 have only been corrected for Rb and Kr, whereas the rightmost sets show the same set of analyses but also corrected for CaCa/CaAr + REE interferences.

The $^{87}Sr/^{86}Sr$ measurements for the three new plagioclase reference materials agree with their reference values and none of the various combinations of molecular or doubly charged REE interference corrections leads to significantly improved accuracy (Fig. 8A). The $^{87}Sr/^{86}Sr$ measurements for G29958 and Hrappsey 14-2 are generally within error of the solution values, with slight negative biases perhaps due to normalisation to AMNH-107160. Different combinations of interference corrections also have little influence on the precision of analyses, with the exception of the addition of the REE^{2+} correction (i.e. Er^{2+} and Yb^{2+}), which increases the uncertainty in $^{87}Sr/^{86}Sr$ for AMNH-107160 and Hrappsey 14-2, likely due to the propagation of error from small signals on half-masses, and is therefore not recommended.

The minimal influence of molecular species on $^{87}Sr/^{86}Sr$ shown in Figure 8A is unsurprising given the small magnitude of these interferences expected for plagioclase (Fig. 4B). To further

evaluate the importance of CaCa/CaAr interferences as a function of plagioclase composition, we compared the baseline subtracted signals of masses 82 and 83 to the anorthite content of the three plagioclase reference materials, which span An54–An90 (Supplementary Figure 1). These signals on masses 82 and 83 do not account for differences in ablation, transport, or ionization efficiencies of the different materials, but it was not possible to normalise the signals due to variable Sr contents in many of the plagioclase reference materials. This comparison demonstrates a subtle positive correlation between increasing anorthite content and total signals on masses 82 and 83, which we interpret to be the result of an increasing contribution of CaCa/CaAr molecules to the signal (Supplementary Figure 1). Despite the concentration of CaCa/CaAr molecules produced across the range of compositions encompassed by the plagioclase reference materials not having a resolvable impact on $^{87}Sr/^{86}Sr$, the general increasing production of CaCa/CaAr molecules with increasing Ca concentration of the analyte may need to be considered when analysing other Ca-rich materials, such as apatite. The generation of NaNi and CaAlO/ArAlO molecules as a function of plagioclase composition was also assessed by monitoring mass 82/83 signals, and no strong correlation with the anorthite content was observed (Supplementary Figure 1). The low concentration of NaNi molecules generated during ablation is unsurprising given that plagioclase crystals sufficiently enriched in Sr for isotopic analysis are likely to be closer to the anorthite endmember of the albite-anorthite solid solution. Similarly, the formation of CaAlO molecules appears to be effectively suppressed by tuning the mass spectrometer to minimise the formation of oxides.

Figure 8B summarises the effect of different combinations of interference corrections on three low Rb/Sr natural rock glass references materials (BIR-1G, KL2, and StHs6/80). Correcting for CaCa/CaAr alone or in combination with CaAlO or NaNi does not significantly improve the accuracy of $^{87}Sr/^{86}Sr$ measurements for any of the rock glass reference materials tested. However, the combined CaCa/CaAr + REE^{2+} correction improves the accuracy of $^{87}Sr/^{86}Sr$ for BIR-1G (88% improvement in accuracy relative to no interference corrections), KL2 (24% improvement), and StHs6/80 (94% improvement), bringing the mean (± 2SD) of the measurements for each reference material into agreement with recommended values. The importance of the REE^{2+} correction for glass and groundmass materials is further highlighted in Figure 8C, which compares the Sr-normalised HREE contents (i.e., (Er+Yb)/Sr) of four low Rb/Sr glass reference materials to the error in $^{87}Sr/^{86}Sr$ measurements prior to REE^{2+} correction and normalisation of $^{87}Sr/^{86}Sr$ to a primary standard. The positive correlation between

560 (Er+Yb)/Sr and error in $^{87}Sr/^{86}Sr$ measurements prior to REE^{2+} peak-stripping evident in Figure
561 8C can likely be attributed to an increasing contribution of doubly charged ^{174}Er and ^{174}Yb ions
562 to the signal on mass 87.
563
564 In summary, Figure 8 illustrates that isobaric interferences are a major source of error for all
565 Sr isotope measurements by LA-MC-ICP-MS and vary in type and magnitude for different
566 geological materials. We focused our systematic testing of interference corrections on
567 plagioclase and mafic to intermediate rock glass reference materials (as a proxy for basaltic to
568 andesitic groundmass) as they are among the most common magmatic materials targeted for
569 Sr isotope analysis. Table 2 summarises recommended interference corrections, bracketing
570 standards, and analytical conditions for plagioclase and groundmass. Although we have not
571 assessed in detail the magnitude of isobaric interferences for the spectrum of geological
572 materials amenable to Sr isotope analysis, we have developed the new *Iolite* data reduction
573 scheme to be as flexible as possible so that users can optimise their data reduction strategy for
574 the target of interest. In addition to allowing users to quickly and systematically test which
575 combination of interference corrections are most suitable for their measurements (Fig. 8), the
576 data reduction scheme can be used to define the proportions of different isobaric interferences
577 (e.g., CaCa vs. CaAr, NaNi vs. CaAlO, or REE ratios) and modify their respective mass-bias
578 factors by scaling βSr.
579
580 ***Residual errors in stable Sr isotope ratios***
581 The stable isotope ratios ($^{84}Sr/^{86}Sr$ and $^{84}Sr/^{88}Sr$) can be used to independently assess the
582 efficacy of interference corrections and instrument mass bias by comparing measured values
583 to the canonical $^{84}Sr/^{86}Sr$ and $^{84}Sr/^{88}Sr$ values of 0.0565 and 0.00675, respectively. However,
584 we have observed large errors (10^4—10^5 ppm, internal 2SE) in $^{84}Sr/^{86}Sr$ and $^{84}Sr/^{88}Sr$ when
585 measuring Sr isotopes in a variety of different materials (plagioclase, glass, apatite, carbonate)
586 via LA-MC-ICP-MS. Similar discrepancies have also been documented in previous LA-MC-
587 ICP-MS studies, but their cause remains unclear. Ramos et al. (2004) observed downhole
588 fractionation of Sr isotopes during ablation of plagioclase using a 213 nm laser, resulting in a
589 progressive lowering of $^{84}Sr/^{86}Sr$ with increasing pit depth, and hypothesised that additional,
590 unknown, interferences on mass 86 could account for the inaccurate $^{84}Sr/^{86}Sr$ values observed
591 in their study. We have not observed downhole fractionation of Sr isotopes using a 193 nm
592 laser (Supplementary Figure 2) and note that despite large errors in $^{84}Sr/^{86}Sr$, the corresponding

593 $^{87}Sr/^{86}Sr$ measurements are accurate, suggesting that interferences on mass 86 cannot be the
594 only cause of bias in stable Sr isotope ratios.
595
596 Kimura et al. (2013) observed correlations between $^{84}Sr/^{86}Sr$, $^{87}Sr/^{86}Sr$, and the signal on mass
597 82, which they attributed to a combination of suppression of Kr baselines by plasma loading
598 (resulting in negative shifts in $^{84}Sr/^{86}Sr$ and positive shifts in $^{87}Sr/^{86}Sr$) and enhancement of
599 baselines from addition of Kr from the sample (resulting in positive shifts in $^{84}Sr/^{86}Sr$ and
600 negative shifts in $^{87}Sr/^{86}Sr$). Uncorrected Kr interferences are an attractive explanation for the
601 observed bias in $^{84}Sr/^{86}Sr$ and $^{84}Sr/^{88}Sr$ measurements because even small contributions from
602 Kr translate to large errors in $^{84}Sr/^{86}Sr$ and $^{84}Sr/^{88}Sr$, yet have comparatively little impact on
603 $^{87}Sr/^{86}Sr$ due to the isotopic abundance of ^{84}Kr (~57.00%) relative to ^{86}Kr (~17.30%) and ^{84}Sr
604 (~0.56%) relative to ^{86}Sr (~9.86%) and ^{88}Sr (~82.58%). For example, a 0.1 mv signal on mass
605 82 due to unsubtracted Kr results in a ~17,000 ppm error for $^{84}Sr/^{86}Sr$ but only a -150 ppm error
606 in $^{87}Sr/^{86}Sr$ (Fig. 9). Similarly, negative biases in stable Sr isotopes of similar magnitude to
607 those outlined in Figure 9 could also arise from baseline suppression of Kr during plasma
608 loading (Kimura et al., 2013).
609
610 Isotopologues of ^{84}(CaAr) (isotopologue abundance ≈ 2.152%) are another potentially
611 important source of interference on ^{84}Sr that could result in inaccurate stable Sr isotope
612 measurements. Our own LA-MC-ICP-MS measurements of stable Sr isotope ratios of
613 plagioclase and glass that are baseline subtracted (i.e., corrected for ^{84}Kr) but not corrected for
614 CaCa/CaAr interferences have large positive errors in $^{84}Sr/^{86}Sr$ and $^{84}Sr/^{88}Sr$ (Supplementary
615 Figure 3). Applying a CaCa/CaAr correction substantially reduces the magnitude of this error
616 but often results in significant overcorrection of both $^{84}Sr/^{86}Sr$ and $^{84}Sr/^{88}Sr$. Such
617 overcorrections could be due to the unconstrained βCaCa/CaAr (assumed to be equivalent to
618 βSr in the new *Iolite* data reduction scheme) or to Kr signal suppression during ablation. The
619 latter can also result in negative $^{84}Sr/^{86}Sr$ and $^{84}Sr/^{88}Sr$ biases. It is difficult to directly calculate
620 βCaCa/CaAr (from Kr-stripped mass 82 and 83 signals, for example) because the measured
621 signals on masses 82 and 83 are typically very low. Therefore, the new *Iolite* data reduction
622 scheme allows users to employ a bias factor (CaArBias) to account for possible differences
623 between βSr and βCaCa/CaAr. Similar to Kr inferences, the error in the radiogenic Sr isotope
624 ratio due to CaCa/CaAr interferences are predicted to be two to three orders of magnitude lower
625 than the error in $^{84}Sr/^{86}Sr$ (Fig. 9). The imprecise stable Sr isotope ratios measured by LA-MC-

ICP-MS therefore do not offer an effective means of assessing the efficacy of interference and mass bias corrections. Instead, we recommended evaluating corrections through accompanying measurements of well-characterised, matrix-matched $^{87}Sr/^{86}Sr$ reference materials.

Influence of spot size and Sr content on measurement precision

The precision of Sr isotope measurements is related to the concentration of Sr in the sample, the mass of material transferred to the mass spectrometer, and the sensitivity (ionisation and transfer efficiency) of the mass spectrometer. This relationship is evaluated for Sr isotope measurements of plagioclase in Figure 10A, which plots the uncertainty of interference-corrected $^{87}Sr/^{86}Sr$ against the apparent Sr concentration of the three new plagioclase reference materials analysed at various spot sizes. Building on the relationship between Sr concentration and precision illustrated in Figure 10A, figures 10B and 10C compare the Sr concentration required for 100 ppm precision on $^{87}Sr/^{86}Sr$ using a 100 µm or 64 µm spot to a compilation of plagioclase Sr concentrations from the GEOROC database (http://georoc.mpch-mainz.gwdg.de/georoc/). For a given analytical spot size, the concentration of Sr in plagioclase and the precision of $^{87}Sr/^{86}Sr$ are described by a power law relationship—as expected due to error dominated by shot noise—with precision improving with increasing Sr concentration to a limit of ~50 ppm (Figure 10A). Precision also improves with increasing spot size at constant Sr concentration, with the greatest improvements observed for materials with lower Sr concentrations (<500 ppm Sr). Rastering the laser beam across a sample provides additional means of improving precision by increasing the volume of material analysed from a domain of interest relative to static spot analyses. Figure 10A shows that rastering a beam with a diameter of 50 µm significantly improves the precision of $^{87}Sr/^{86}Sr$ for materials with <1000 Sr ppm relative to a 50 µm static spot. In contrast, little improvement in precision is observed for a 100 µm raster relative to 100 µm spot analysis, regardless of Sr content (Fig. 10A). Therefore, rastering samples with a small beam diameter may be a useful approach for small or texturally complex crystals (see case study below). Rastering also reduces the depth of ablated sample relative to spot analyses, which may be desirable for samples that are subject to additional LA-ICP-MS analyses (e.g., elemental mapping; Ubide et al., 2015).

Ideally, the Sr concentration of minerals would be characterised prior to Sr isotope analysis so that an appropriate spot size can be selected with reference to the relationship outlined in Figure 10A. In cases where prior quantification of Sr concentration is not possible, the compilation of

Sr concentrations for plagioclase summarised in Figure 10B or the relationship between anorthite content and Sr concentration shown in Figure 10C may provide a useful reference for anticipating the required analytical spot size. Based on the analysis outlined in Figure 10, we suggest that a 100 μm static spot should provide a suitable balance between spatial resolution and precision for *in situ* Sr isotope measurements for minerals with low to moderate Sr contents such as plagioclase with (<500—1000 ppm Sr). For these minerals, a 100 μm static spot analysis can achieve 100 ppm precision on $^{87}Sr/^{86}Sr$, which can resolve Sr isotope variations in magmatic systems (e.g., Hagen-Peter et al., 2019). For geological materials with lower Sr contents such as clinopyroxene (typical Sr content of < 100 ppm; Zhao et al. 2020) or basaltic groundmass, and to resolve fine features in plagioclase crystals, rastering may be used to achieve suitable precision while maintaining high spatial resolution, as illustrated in the case study below.

Case Study: Plagioclase crystals and groundmass from Merapi Volcano

Plagioclase phenocrysts are ubiquitous in arc andesites, and their texture and composition provide excellent records of magmatic histories preceding eruption (Davidson et al., 2007; Cashman and Blundy, 2013). Complementing crystal archives, groundmass geochemistry records the composition of the carrier melt (Magee et al., 2021), without the complicating effects of crystal accumulation inherent to whole rock geochemical data (Ubide et al., 2022). Here, we resolve the Sr isotope compositions in plagioclase and groundmass in a sample from the pyroclastic deposits of the 2010 eruption at Merapi volcano, Indonesia (previously described by Costa et al., 2013). The 2010 eruption was much larger and more explosive than most dome-forming eruptions of the past century. The increase in explosivity in 2010 has been linked to gas overpressure due to either 1) contamination with crustal carbonates, increasing magmatic CO_2 contents (Borisova et al., 2013; 2016; Troll et al., 2012); or 2) rapid ascent of relatively undegassed magma (Handley et al., 2018) before the eruption. As a robust tracer of crustal assimilation and mixing of magmatic reservoirs, radiogenic Sr isotopes may provide new insight into the mechanisms driving the onset of explosive volcanism.

The sample of the pyroclastic deposits of the 2010 eruption at Merapi provides an ideal case study to examine the analytical and data reduction protocols outlined here (Fig. 11). Plagioclase phenocrysts preserve complex internal textures and fine compositional zoning, which would

692 be difficult to sample via micromilling. Furthermore, the microcrystalline groundmass (with
693 microlites of plagioclase, two pyroxenes, apatite and magnetite, and limited interstitial glass;
694 Costa et al., 2013) provides an opportunity to test the efficacy of molecular and elemental
695 interference corrections for a compositionally diverse medium, which can be compared to
696 whole rock TIMS Sr isotope data from the same eruption (Handley et al., 2018). In addition,
697 Chadwick et al. (2007) measured the Sr isotopic composition of groundmass and plagioclase
698 megacrysts from avalanche products of the 1998 eruption of Merapi via micromilling + TIMS,
699 allowing for a comparison of solution- and laser ablation-based techniques on nominally
700 similar geological materials.
701
702 LA-MC-ICP-MS Sr isotopes measurements were performed on a standard polished thin section
703 of Merapi 2010 andesite at The University of Queensland, using the analytical method and data
704 reduction approach outlined above and the micro-sampling strategy illustrated in Fig. 11. Two
705 representative plagioclase crystals were selected for detailed Sr isotope measurements, which
706 were performed using rasters with a 65 μm spot diameter placed in distinct textural-
707 compositional domains within each crystal. A further ten plagioclase crystals were selected for
708 statistic spot analysis using a 100 μm spot diameter, placed in texturally homogenous core
709 domains. The rock groundmass was analysed using rasters with a 100 μm spot diameter, with
710 care taken to avoid ablating phenocrysts. Plagioclase crystals and groundmass were analysed
711 in separate analytical sessions. Each session lasted approximately 6 hours and adopted
712 standard-sample bracketing in which blocks of 10–15 analyses of unknowns were separated by
713 a standard bracket comprising two analyses of a primary reference material (AMNH-10760 for
714 plagioclase, BHVO-2G for groundmass), two analyses of BCR-2G for calculating βRb-βSr
715 offset, and two analyses of multiple secondary reference materials (G29958 and Hrappsey 14-
716 2 for plagioclase; BIR1-G, KL2-G, and StHs6/80-G for groundmass). Interference corrections
717 follow those outlined in Table 2 and analytical results are presented in Supplementary File 5.
718
719 The results of the LA-MC-ICP-MS Sr isotope measurements are summarised in their textural
720 and compositional context in Figure 11. The Ca map in Figure 11A was obtained at the
721 Australian Synchrotron X-ray fluorescence microscopy beamline (details described in Magee
722 et al., 2021), and highlights the abundance of small (~1 mm) plagioclase phenocrysts with
723 complex zoning patterns across the sample. Sr isotope measurement locations are shown in a
724 reflected light scan of the thin section in Figure 11B. The key textural and compositional

characteristics of representative plagioclase crystals are summarised in Figure 11C—F. Plagioclase crystals from the 2010 eruption are characterised by three distinct textural-compositional domains: (1) anhedral, low-anorthite (An) inner cores surrounded along sharp contacts by (2) euhedral, high-An core domains, which are in turn surrounded by (3) oscillatory zoned rims that record a rim-ward decrease in An (Fig. 11E and 11F and 11I and 11J). The $^{87}Sr/^{86}Sr$ composition of these three textural-compositional domains are indistinguishable within uncertainty from one another and from the surrounding groundmass (Fig. 11G and 11H). The homogeneity of Sr isotopes in this sample is further reinforced by the 10 static spot analyses (100 μm diameter) of plagioclase grains, which yielded $^{87}Sr/^{86}Sr$ values that also overlap the $^{87}Sr/^{86}Sr$ composition of the groundmass (Fig. 11K).

A comparison of the new LA-MC-ICP-MS Sr isotope measurements of plagioclase and groundmass from the Merapi 2010 eruption, whole rock TIMS Sr isotope data from the same eruption reported by Handley et al. (2018), and micromilled + TIMS Sr isotope measurements of plagioclase and groundmass from the 1998 eruption of Merapi reported by Chadwick et al. (2007) is summarised in Figure 11K. The plagioclase megacrysts from the 1998 eruption studied by Chadwick et al. (2007) are considerably larger than those from the 2010 eruption (>2 mm and <1.5 mm, respectively) but preserve textural and compositional characteristics comparable to the three distinct domains observed in the 2010 plagioclase crystals (Fig. 11E and 11F).

Despite their similar textural features and elemental concentrations, the plagioclase crystals from the 1998 and 2010 eruptions of Merapi have differing Sr isotope systematics. Although the new LA-MC-ICP-MS data reported from 2010 plagioclase crystals are less precise than TIMS data from 1998 eruption, the up to 800 ppm variations in $^{87}Sr/^{86}Sr$ (total variation is beyond the range of the y-axis in Fig. 11K) between the different the textural-chemical domains reported by Chadwick et al. (2007) are not observed in plagioclase crystals from the 2010 eruption. This is despite variations of this magnitude being well within the range resolvable by the new LA-MC-ICP-MS measurements during the analytical session (~150 ppm 2SE). In addition to the differing Sr isotope systematics of plagioclase crystals, the groundmass Sr isotope composition of the two eruptions also differs with the Sr isotopic composition of the 1998 eruption (~0.705800—0.705950) being distinctly higher than that of the 2010 eruption (~0.705675—0.705775). Our new groundmass data is in good agreement with the whole rock

TIMS results of Handley et al. (2018), further demonstrating isotopic equilibrium between crystals and the carrier melt.

The contrasting Sr isotope systematics with respect to textural and chemical domains suggests that plagioclase crystals from the 1998 and 2010 eruptions of Merapi formed through different processes. Two simplified petrogenetic models accounting for the differing Sr isotopic systematics of the 1998 eruption (Chadwick et al., 2007) and the 2010 eruption (this study) are summarised in Figure 11L and 11M. Chadwick et al. (2007) interpreted high-An and high-$^{87}Sr/^{86}Sr$ euhedral plagioclase cores to represent xenocrysts derived from assimilation of wallrock carbonates. This interpretation is supported by the presence of calc-silicate xenoliths with high $^{87}Sr/^{86}Sr$ (0.707866) that are also found in deposits from the 1998 eruption. Chadwick et al. (2007) interpreted the overgrowth of the high-An, high $^{87}Sr/^{86}Sr$ xenocrysts cores by domains with lower An and $^{87}Sr/^{86}Sr$ to reflect the continued growth of plagioclase from a wallrock-contaminated melt, which may also fill in the cracks and pore space generating low An and low $^{87}Sr/^{86}Sr$ anhedral cores. Assimilation of wallrocks by ascending melts is supported by the $^{87}Sr/^{86}Sr$ signature of the 1998 groundmass, which is more radiogenic than the 2010 groundmass (Fig. 11K).

In contrast, a petrogenetic model for the 2010 Merapi eruption must account for the same textural and compositional features of plagioclase crystals but without significant changes in the Sr isotopic composition of the host melt. The lack of resolvable intra- or inter-crystal Sr isotopic variation in plagioclase crystals suggests that assimilation of wallrock carbonate was not important during the 2010 eruption of Merapi. Instead, we propose high-An cores crystallised from H_2O-rich, basaltic magmas at depth, and low-An rims and infills crystallised due to magma degassing and fractional crystallisation upon ascent above the H_2O-saturation level. High dissolved H_2O contents in melts increase the An content of equilibrium plagioclase, such that An-rich plagioclase phenocrysts are common in arc-related, typically hydrous basaltic magmas (Wallace et al., 2015). In the 2010 phenocrysts, high-An cores have euhedral habits, supporting a cogenetic origin with the host magma. The high-An cores testify to mafic, undegassed magma recharging the plumbing system prior to eruption. This agrees with an eruption trigger via rapid recharge of high volumes of mafic, undegassed magma from depth, as suggested by petrological information (Costa et al., 2013) and U-series disequilibria (Handley et al., 2018) on the 2010 eruptive products. Our results support the notion that

injections of cogenetic, undegassed magma may lead to explosive eruptions without the need of a CO_2 input via carbonate assimilation as inferred for the 1998 eruption by Chadwick et al. (2007).

This case study highlights the effectiveness of the LA-MC-ICP-MS technique to resolving $^{87}Sr/^{86}Sr$ variations across crystal zones and populations in representative sample sets. The LA-MC-ICP-MS analytical and data reduction protocols outlined in this study can produce accurate and precise Sr isotopic data to unveil magmatic histories recorded in crystals of varied sizes and from numerous thin sections or resin mounts. Although solution-based analyses remain the benchmark for resolving small-scale isotopic heterogeneity, the key advantage of the LA-MC-ICP-MS technique is the speed and high spatial resolution of analyses, which facilitate a greater number of measurements and sampling of small-scale textural or compositional domains, ultimately providing more representative isotopic datasets. The distinct petrogenetic models inferred from integrating textural, compositional, and Sr isotope data from plagioclase crystals from two separate eruptions of Merapi Volcano highlight the complexity of natural magmatic systems, offering a more holistic view of the secular evolution of magma processes and volcanic behaviour.

CONCLUSIONS AND RECOMMENDATIONS

The radiogenic Sr isotope system can be measured in many common rock-forming minerals, accessory phases, and groundmasses, and hence can record a diverse range of magmatic, volcanic, and hydrothermal processes. We outline a series of analytical procedures and data reduction strategies to facilitate *in-situ* Sr isotope measurements by LA-MC-ICP-MS. Thanks to the high spatial resolution of this technique, even small individual crystal zones or groundmass domains can be targeted for Sr isotope analysis. The ease of sample preparation and rapid analysis allow hundreds of measurements to be undertaken in a single day. Therefore, the LA-MC-ICP-MS method outline here can routinely produce representative $^{87}Sr/^{86}Sr$ data within individual samples and across samples, with uncertainties of better than 100 ppm.

To assist in addressing inconsistencies in the selection of standards and assessing interference corrections, we developed practical analytical procedures and data reduction strategies by

analysing a series of newly characterised plagioclase reference materials and widely available rock glass reference materials. Based on our results, we offer the following recommendations for collecting and reporting *in situ* Sr isotope data by LA-MC-ICP-MS (Table 2; Fig. 10):

(1) Although it has been common practice to use carbonate or rock glasses in place of matrix-matched standards (Fig. 2), matrix-matched reference materials are now available for most magmatic minerals commonly analysed for Sr isotopes including plagioclase (this study), apatite (Yang et al., 2014; Apen et al., 2022), and clinopyroxene (Zhao et al. 2020), and should be included as an integral component of *in situ* Sr isotope analytical protocols.

(2) LA-MC-ICP-MS stable Sr isotope measurements ($^{84}Sr/^{86}Sr$ and $^{84}Sr/^{88}Sr$) are imprecise and may have large biases relative to canonical values due the typically very low signals on mass 84 and possible isobaric interferences from ^{84}Kr and ^{84}(CaAr). However, these interferences generally do not have a significant impact on $^{87}Sr/^{86}Sr$ measurements. Therefore, the efficacy of interference and mass bias corrections for Sr isotope measurements by LA-MC-ICP-MS are best evaluated through standard-sample bracketing with well-characterised $^{87}Sr/^{86}Sr$ reference materials.

(3) Analysis with a 100 μm spot generates a suitable signal to achieve a 2SE of ~100 ppm in $^{87}Sr/^{86}Sr$ for materials with moderate Sr concentrations (<500—1000 ppm). Rastering can improve the precision relative to spot analysis, with the greatest improvement at smaller spot sizes (~50 μm).

We developed a new data reduction scheme for *Iolite* (Supplementary File 3) that can apply a variety of common interference corrections inherent to *in situ* Sr isotope measurements:

(1) On-peak baseline subtraction provides a simple means of correcting for Kr interferences from the ICP and carrier gas. The alternative approaches for Kr correction outlined by Kimura et al. (2013) and Konter & Storm (2014) are viable alternatives, but may be less practical than on-peak baseline subtraction.

(2) Standard-sample bracketing with a reference material with moderate Rb/Sr (e.g., BCR-2G glass) provides a simple way to directly constrain βRb, which improves the efficacy of ^{87}Rb interference corrections. We prefer this approach over the assumption that $\beta Sr = \beta Rb$ for all materials, and particularly for materials with moderate Rb/Sr such as

groundmass or clinopyroxene. Materials with Rb/Sr >0.30 may not produce accurate results and are not recommended for *in situ* Sr-isotope analysis by LA-MC-ICP-MS.

(3) The generation of NaNi, CaAlO, or CaCa/CaAr molecules did not introduce significant bias (i.e., correcting for them did not significantly affect the $^{87}Sr/^{76}Sr$) in our analyses of plagioclase and rock glass reference materials. Nevertheless, the magnitude and type of molecular interference (i.e. NaNi vs. CaAlO or CaCa vs. CaAr) can monitored on signals on masses 82 and 83 and stripped from Sr isotope signals, as necessary.

(4) Doubly charged REE interferences can be a significant source of error for materials with elevated Er + Yb concentrations, notably apatite. The REE^{2+} correction may also be important in analysing low-Sr materials requiring large spot sizes or rasters to achieve suitable precision (Fig. 11), which increases the chance of inadvertently ablating small REE-enriched phases. Contributions of REE^{2+} from REE-rich phases can be monitored on signals on the half masses 83.5, 86.5, and 87.5 on many typical Faraday detector arrays. This correction is not recommended in plagioclase or other materials with low REE contents as it decreases precision without improving in accuracy.

Although these recommendations provide a general guideline for measuring radiogenic Sr isotopes by LA-MC-ICP-MS, the most effective approach will likely differ between laboratories, instruments, and even day-to-day as tuning conditions change. Our new reference materials, analytical protocols, and data reduction strategies aim to facilitate a more standardised approach to collecting, correcting, and reporting *in situ* Sr isotope measurements by LA-MC-ICP-MS and encourage the continued development and application of the technique to understanding Earth systems.

ACKNOWLEDGEMENTS

TU acknowledges funding from a Foundation Research Excellence Award from The University of Queensland (UQ-FREA RM2019001828), the Advance Queensland Women's Research Assistance Program from the Queensland Government (WRAP109-2019RD1 RM2020002371), the Australian Synchrotron, part of ANSTO (X-ray fluorescence microscopy beamline experiment AS183/XFM/13961 RM2018002281), and AuScope (National Research Infrastructure for Australia). CEL and CT acknowledge funding from the Danish National Research Foundation, the Carlsberg Foundation and Aarhus University. This is Vegacenter

publication #XXX. We thank the American Museum of Natural History and the Swedish Museum of Natural History for sourcing the plagioclase reference materials.

REFERENCES

Apen, F.E., Wall, C.J., Cottle, J.M., Schmite, M.D., Kylander-Clark, A.R., and Seward, G.G., (2022). Apatites for destruction: Reference apatites from Morocco and Brazil for U-Pb petrochronology and Nd and Sr isotope geochemistry. Chemical Geology, 590, 120689.

Bevan, D., Coath, C. D., Lewis, J., Schwieters, J., Lloyd, N., Craig, G., Wehrs, H., Elliott, T. (2021). In situ Rb–Sr dating by collision cell, multicollection inductively-coupled plasma mass-spectrometry with pre-cell mass-filter (CC- MC-ICPMS/MS). Journal of Analytical Atomic Spectrometry, 36, 917–931.

Bolea-Fernandez, E., Van Malderen, S. J., Balcaen, L., Resano, M., & Vanhaecke, F. (2016). Laser ablation-tandem ICP-mass spectrometry (LA-ICP-MS/MS) for direct Sr isotopic analysis of solid samples with high Rb/Sr ratios. Journal of Analytical Atomic Spectrometry, 31, 464–472.

Borisova, A.Y, Martel, C., Gouy, S., Indyo Pratomo, I., Sumarti, S., Toutain, J.-P., Bindeman, I.N., de Parseval, P., Metaxian, J.-P., Surono, M. (2013). Highly explosive 2010 Merapi eruption: evidence for shallow-level crustal assimilation and hybrid fluid. Journal of Volcanology and Geothermal Research, 261, 193–208.

Borisova A.Y., Gurenko A. A., Martel C., Kouzmanov K., Cathala A., Bohrson W.A., Pramoto I. and Sumarti S. (2016). Oxygen isotope heterogeneity of arc magma recorded in plagioclase from the 2010 Merapi eruption (Central Java, Indonesia). Geochimica et Cosmochimica Acta, 190, 13–34.

Brennan S.R., Zimmerman C.E., Fernandez D.P., Cerling T.E., McPhee M.V., and Wooller M.J. (2015). Strontium isotopes delineate fine-scale natal origins and migration histories of Pacific salmon. Science Advances, 1, e1400124–e1400124.

Cashman, K., and Blundy, J. (2013). Petrological cannibalism: the chemical and textural consequences of incremental magma body growth. Contributions to Mineralogy and Petrology, 166, 703–729.

Chadwick, J.P., Troll, V.R., Ginibre, C., Morgan, D., Gertisser, R., Waight, T.E., and Davidson, J.P. (2007). Carbonate assimilation at Merapi Volcano, Java, Indonesia: insights from crystal isotope stratigraphy. Journal of Petrology, 48, 1793–1812.

Charlier, B. L. A., Ginibre, C., Morgan, D., Nowell, G. M., Pearson, D. G., Davidson, J. P. and Ottley, C. J. (2006). Methods for the microsampling and high-precision analysis of strontium and rubidium isotopes at single crystal scale for petrological and geo-chronological applications. Chemical Geology 232, 114–133.

Christensen J. N., Halliday A. N., Lee D. C., and Hall C. M. (1995) In-situ Sr isotopic analysis by laser-ablation. Earth and Planetary Science Letters, 136(1–2), 79–85

Cho, J. O., Scoates, J. S., Weis, D., Amini, M., (2022). Lead isotope geochemistry of plagioclase in the Skaergaard intrusion by LA-ICP-MS: Assessing the effects of crustal contamination and link with East Greenland flood basalts. Chemical Geology, 592, 120723.

Costa, F., Andreastuti, S., Bouvet de Maisonneuve, C., Pallister, J. S. (2013). Petrological insights into the storage conditions, and magmatic processes that yielded the centennial 2010 Merapi explosive eruption. Journal of Volcanology and Geothermal Research, 261, 209–235.

Davidson, J. P., Morgan, D. J., Charlier, B. L. A., Harlou, R. and Hora, J. M. (2007) Microsampling and isotopic analysis of igneous rocks: implications for the study of magmatic systems. Annual Review of Earth and Planetary Sciences, 35, 273–311.

Davidson J., Tepley F., Palacz Z., and Meffan-Main S. (2001) Magma recharge, contamination and residence times revealed by in situ laser ablation isotopic analysis of feldspar in volcanic rocks. Earth and Planetary Science Letters, 184(2), 427–442.

Edwards, M. A., Jackson, M. G., Kylander-Clark, A. R. C., Harvey, J., Hagen-Peter, G. A., Seward, G. G. E., et al. (2019) Extreme enriched and heterogeneous 87Sr/86Sr ratios recorded in magmatic plagioclase from the Samoan hotspot. Earth and Planetary Science Letters, 511, 190–201.

Gillespie J., Nemchin A.A., Kinny P.D., Martin L., Aleshin M., Roberts M.P., Ireland T.R., Whitehouse M.J., Jeon H., Cavosie A.J. and Kirkland C.L. (2021) Strontium isotope analysis of apatite via SIMS. Chemical Geology, 559, 119979.

Griffin, J. M., Montañez, I. P., Glessner, J. J. G., Chen, J., and Willmes, M. (2021). Geologic variability of conodont strontium isotopic composition quantified by laser ablation multiple collection inductively coupled plasma mass spectrometry. Palaeogeography, Palaeoclimatology, Palaeoecology, 568:110308.

Hagen-Peter, G., Tegner, C., and Lesher, C.E. (2019) Strontium isotope systematics for plagioclase of the Skaergaard intrusion (East Greenland): a window to crustal assimilation, differentiation, and magma dynamics. Geology, 47, 313–316.

Handley, H. K., Reagan, M., Gertisser, R., Preece, K., Berlo, K., McGee, L. E., Barclay, J., and Herd, R. (2018). Timescales of magma ascent and degassing and the role of crustal assimilation at Merapi volcano (2006–2010), Indonesia: Constraints from uranium-series and radiogenic isotopic compositions. Geochimica et Cosmochimica Acta, 222, 34–52.

Horstwood, M.S.A., Košler, J., Gehrels, G., Jackson, S.E., McLean, N.M., Paton, C., Pearson, N.J., Sircombe, K., Sylvester, P., Vermeesch, P., Bowring, J.F., Condon, D. J., and Schoene, B. (2016) Community-derived standards for LA-ICP-MS U-Th-Pb geochronology – uncertainty propagation, age interpretation and data reporting. Geostandards and Geoanalytical Research, 40, 311–33.

975 Hepworth, L. N., Daly, J. S., Gertisser, R., Johnson, C. G., Emeleus, C. H. and O'Driscoll, B.
976 (2020) Rapid crystallization of precious-metal-mineralized layers in mafic magmatic systems.
977 Nature Geoscience, 13, 375–377
978
979 Jackson, M.G., and Hart, S.R., (2006) Strontium isotopes in melt inclusions from Samoan
980 basalts: implications for heterogeneity in the Samoan plume. Earth and Planetary Science
981 Letters, 245, 260–277.
982
983 Jeon, H., Whitehouse, M.J. (2021). A Robust LG-SIMS method for Sr isotope
984 determination in apatite across a wide Sr concentration range. Geostandards and
985 Geoanalytical Researcg, 45, 325–340.
986
987 Jochum K.P., Stoll B., Weis U., Kuzmin D.V. and Sobolev A.V. (2009) In situ Sr isotopic
988 analysis of low Sr silicates using LA-ICP-MS. Journal of Analytical Atomic Spectrometry,
989 24, 1237–1243.

990 Kemp, A.I.S., and Hawkesworth, C.J., (2013) Growth and differentiation of the continental
991 crust from isotope studies of accessory minerals. In: Rudnick, R.L. (Ed.), Treatise On Geo-
992 chemistry, 2nd ed. The Crust vol. 12. Elsevier Science, Oxford.

993 Kimura, J.-I., Takahashi, T., and Chang, Q. (2013) A new analytical bias correction for in situ
994 Sr isotope analysis of plagioclase crystals using laser-ablation multiple-collector inductively
995 coupled plasma mass spectrometry. Journal of Analytical Atmoic Spectrometry, 28, 945–957.
996
997 Konter, J.G. and Storm, L.P. (2014) High precision 87Sr/86Sr measurements by MC-ICP-
998 MS, simultaneously solving for Kr interferences and mass-based fractionation. Chemical
999 Geology, 385, 26–34.
1000
1001 Kristmannsdottir, H. (1971). Anorthosite inclusions in Tertiary dolerite from the island
1002 groups Hrappsey and Purkey, West Iceland. The Journal of Geology, 79, 741–748.
1003
1004 Magee, R., Ubide, T., Caulfield, J. (2021) Days to weeks of syn-eruptive magma interaction:
1005 High-resolution goechemistry of the 2002-03 branched eruption at Mount Etna. Earth and
1006 Planetary Science Letters, 565, 116904.
1007

1008 Mulder, J.A., Halpin, J.A., Daczko, N.R., Orth, K., Meffre, S., Thompson, J.M., Morrissey,
1009 L.J. (2019). A Multiproxy provenance approach to uncovering the assembly of East
1010 Gondwana in Antarctica. Geology, 47, 645–649.

1011 Muller W. and Anczkiewicz R. (2016) Accuracy of laser-ablation (LA)-MC-ICP-MS Sr
1012 isotope analysis of (bio) apatite – A problem reassessed. Journal of Analytical Atomic
1013 Spectrometry, 31, 259–269.
1014
1015 Paton C., Woodhead J.D., Hellstrom J.C., Hergt J.M., Greig A. and Maas R. (2010) Improved
1016 laser ablation U-Pb zircon geochronology through robust downhole fractionation correction.
1017 Geochemistry Geophysics Geosystems, 11, 1–36.
1018

Pin, C., D. Briot, C. Bassin, and F. Poitrasson. (1994) Concomitant separation of strontium and samarium-neodymium for isotopic analysis in silicate samples, based on specific extraction chromatography, Analytica Chimica Acta, 298, 209–217.

Ramos, F.C., Wolff, J.A., Tollstrup, D.L. (2004) Measuring 87Sr/86Sr variations in minerals and groundmass from basalts using LA-MCICPMS. Chemical Geology, 211, 135–158.

Rösel, D., and Zack, T. (2021) LA-MS/MS Single-Spot Rb-Sr Dating. Geostandards and Geoanalytical Research, 46, 143–168.

Tong, X.R., Liu, Y.S., Hu, Z.C., Chen, H.H., Zhou, L., Hu, Q.H., Xu, R., Deng, L.X., Chen, C.F., Yang, L., and Gao S. (2016) Accurate determination of Sr isotopic compositions in clinopyroxene and silicate glasses by LA-MC-ICP-MS. Geostandards and Geoanalytical Research, 40 (1), 85–99.

Troll, V.R., Hilton, D.R., Jolis, E.M., Chadwick, J.P., Blythe, L.S., Deegan, F.M., Schwarzkopf, L.M., Zimmer, M. (2012). Crustal CO2 liberation during the 2006 eruption and earthquake events at Merapi volcano, Indonesia. Geophysical Research Letters, 39, L11302

Ubide, T., McKenna, C.A., Chew, D.M., and Kamber, B.S. (2015) High-resolution LA-ICP-MS trace element mapping of igneous minerals: in search of magma histories. Chemical Geology, 409, 157–168.

Ubide, T., Larrea, P., Becerril, L. and Gale, C. (2022). Volcanic plumbing filters on ocean-island basalt geochemistry. Geology, 50, 26–31.

Van Ham-Meert, A., Chernonozhkin, S., Van Malderen, S.J.M., Van Acker, T., Vanhaecke, F., and Degryse, P. (2018). Assessment of nanosecond Laser Ablation Multi-collector-inductively Coupled Plasma-mass Spectrometry for Pb and Sr isotopic analysis of archaeological glas – mass bias correction strategies and results for Corning glass Reference materials. Geostandards and Geoanalytical Resesarch, 42, 223–238.

Vroon, P.Z., van der Wagt, B., Koornneef, J.M., and Davies, G.R. (2008). Problems in obtaining precise and accurate Sr isotope analysis from geological materials using laser ablation MC–ICPMS. Analytical and Bioanalytical Chemistry, 390, 465–476.

Wallace, P.J., Plank, T., Edmonds, M., Hauri, E.H. (2015). Volatiles in magmas. In: The Encyclopedia of Volcanoes. Academic Press, p. 163–183.

Weis D., Kieffer B., Maerschalk C., Barling J., de Jong J.,Williams G.A., Hanano D., Pretorius W., Mattielli N.,Scoates J.S., Goolaerts A., Friedman R.M. and MahoneyJ.B. (2006) High-precision isotopic characterization of USGS referencematerials by TIMS and MC-ICP-MS.Geochemistry Geo-physics Geosystems,7, Q08006

Willmes, M., K. M. Ransom, L. S. Lewis, C. T. Denney, J. J. G. Glessner, and J. A. Hobbs. (2018). IsoFishR: an application for reproducible data reduction and analysis of strontium isotope ratios ($^{87}Sr/^{86}Sr$) obtained via laser-ablation MC-ICP-MS. PLoS One, 13:e204519.

Woodhead J.D., Swearer S., Hergt J. and Maas R. (2005) In situ Sr-isotope analysis of carbonates by LA-MC-ICP-MS: Interference corrections, high spatial resolution and an example from otolith studies. Journal of Analytical Atomic Spectrometry, 20, 22-27.

Xu, L., Yang, J. H., Wang, H., Li, Y., Zhou, B. Q., Yang, Y. H., ... & Wu, S. T. (2022). A natural plagioclase reference material for microbeam Sr isotopic analysis. Journal of Analytical Atomic Spectrometry, 37, 1706-1714.

Yang, Y.H., Wu, F.Y., Yang, J.H., Chew, D.M., Xie, L.W., and Chu, Z.Y. (2014) Sr and Nd isotopic compositions of apatite reference materials used in U–Th–Pb geochronology. Chemical Geology 385, 35–55.

Zack, T., and Hogmalm, K. J. (2016) Laser ablation Rb/Sr dating by online chemical separation of Rb and Sr in an oxygen-filled reaction cell. Chemical Geology, 437, pp. 120–133.

Zhang, L., Ren, Z.-Y., Wu, Y.-D., and Li, N. (2018) Strontium isotope measurement of basaltic glasses by laser ablation multiple collector inductively coupled plasma mass spectrometry based on a linear relationship between analytical bias and Rb/Sr ratios. Rapid Communications in Mass Spectrometry, 32, 105–112.

Zhao, H., Zhao, X.M., and Roux, P.J. (2020) Natural Clinopyroxene Reference Materials for in situ Sr Isotopic Analysis via LA-MC-ICP-MS. Frontiers in Chemistry, 8, 594316.

FIGURE CAPTIONS

Figure 1

Comparison of the number of studies presenting *in situ* Sr isotope data from plagioclase measured by laser ablation multi-collector mass spectrometry (LA-MC-ICP-MS; purple) or micromilling and thermal ionisation mass spectrometry (TIMS) or solution-based MC-ICP-MS (orange) published over the past three decades. Purple bars show the percentage of studies each year that used LA-MC-ICP-MS. Data sourced from Clarivate Web of Science database using the search term 'Sr isotope plagioclase'.

Figure 2

Summary of the type of secondary standards, stable isotope ratios, and molecular interference corrections reported for 65 studies presenting LA-MC-ICP-MS Sr isotope measurements of plagioclase published of the past three decades. Data sourced from Clarivate Web of Science database using the search terms 'Sr isotope plagioclase'.

Figure 3

Isotopic abundance and composition of species relevant to Sr isotope analyses. (A) Isotopic abundances of Sr isotopes and interfering species across the mass/charge ratio (m/z) range 82–88. There are multiple interferences on Sr isotopes and on other interfering elements, which require multiple iterations of peak-stripping to remove. (B) Percent of total isotopes (and isotopologues of Ca-bearing molecules) of Sr and interfering species on masses 82–88. (C) Schematic diagram showing the maximum abundance of interfering species on Sr isotopes during analysis of plagioclase. The left column shows the representative concentration of relevant elements, and the right-hand column shows the concentration of these elements across the mass range 82–88 (derived from the isotopic abundances shown in panel B). Note that the Ca concentration is not to scale and the concentration of Rb and REE species are combined for clarity (e.g., plagioclase Er + Yb + Rb = 1.5 ppm). The diagram highlights, for example, that although Ca is the most abundant species capable of producing isobaric interferences during Sr isotope analysis of plagioclase, only ~3% of all CaCa/CaAr molecules yield m/z ratios that produce isobaric interferences. In contrast, Rb concentration is

low in plagioclase but theoretically, 100% of measured Rb ions have m/z of 82–88. The true abundance of the molecular and doubly charged species measured will realistically be much lower as not all atoms of the elements will form these species.

Figure 4

Simulations of various interferences, and other measurement errors, on Sr isotope ratios for a hypothetical measurement of a sample with $^{87}Sr/^{86}Sr = 0.710000$ and 0.5 V signal for ^{86}Sr. The grey shaded area on the x-axis of panels A, B, and C shows the typical on-peak electronic-baseline-subtracted signal or ratio measured for plagioclase during this study. (A) Error in $^{87}Sr/^{86}Sr$ resulting from unsubtracted Kr signals of similar magnitude to those observed during on-peak baselines (above the electronic baseline). Calculations account for direct interferences on the Sr isotope ratios and the effect on the Sr mass-bias factor. Inset compares electronic and on-peak baseline signals on mass 83 during a typical plagioclase analysis. (B) Error in $^{87}Sr/^{86}Sr$ versus signal on mass 82 (for CaCa/CaAr interferences) or 83 (for NaNi and CaAlO interferences). (C) Error in $^{87}Sr/^{86}Sr$ due to the interference of ^{87}Rb on ^{87}Sr. Inset shows errors in age-corrected $^{87}Sr/^{86}Sr$ arising from elemental fractionation of Sr and Rb during a laser-ablation measurement. Calculations assume 30% fractionation between Rb-Sr (i.e., the measured Rb/Sr is 30% higher than "true" ratio), which was typical of that observed in measurements of rock glass standards in this study. (D) Error in $^{87}Sr/^{86}Sr$ due to unaccounted differences in mass fractionation between Sr and Rb. Grey shaded area on x-axis shows the percent difference between βSr and βRb constrained by analyses of BCR-2G during this study. (E) Error in $^{87}Sr/^{86}Sr$ due to interferences from doubly charged HREE (Er^{2+}, Yb^{2+}, Lu^{2+}). Errors are simulated for a material with a chondritic Er/Yb and Er/Lu and the Madagascar apatite reference material (Er/Yb = ~1.4, Er/Lu = ~11; Yang et al., 2014). Grey shaded area on x axis shows typical signals on mass 83.5 (a proxy for $^{167}Er^{2+}$) measured for basaltic glass (<0.15 mV) and apatite (<0.5 mV).

Figure 5

Summary of the significance of doubly charged REE interferences for geological materials commonly targeted for Sr isotope measurements. (A) Histogram of the Er+Yb content of apatite, carbonate, clinopyroxene, and plagioclase. Data sourced from the GEOROC database: http://georoc.mpch-mainz.gwdg.de/georoc/. Inset in the main panel shows typical

chondrite normalised REE patterns for different geological materials. Er and Yb are marked with dashed vertical lines. Plot below shows detail of the x axis and highlights that plagioclase, carbonate, and clinopyroxene typically have Er + Yb <10 ppm. Apatite distribution is not plotted for clarity. Dashed vertical line shows Er + Yb contents of BCR-2G glass reference material as a proxy for basaltic groundmass. (B) Typical signals measured on mass 83.5 (a proxy for $^{167}Er^{2+}$) during ablation of apatite (Durango and Madagascar), basaltic glass (BCR-2G), carbonate (a modern mollusc shell), and plagioclase (AMNH-10760). (C) Deviation of $^{87}Sr/^{86}Sr$ for different materials relative to recommended values with and without corrections for doubly charged REE. The individual bars represent deviation in ppm (± 2SE, internal) of the measured ratio relative to the recommended value of the ratio. The $^{87}Sr/^{86}Sr$ measurements are corrected for Kr, Rb, and CaCa/CaAr interferences but are not normalised to a primary standard. The REE^{2+}-correction is required to obtain accurate results in materials with high concentrations in Er+Yb (e.g., apatite). In contrast, the REE^{2+}-correction is not recommended for materials with low Er+Yb contents (e.g., plagioclase measurements are generally more accurate and precise without the REE^{2+} correction).

Figure 6

Solution MC-ICP-MS and TIMS data for the three new plagioclase reference materials. Black-filled circles represent the first measurement of a given fragment, with duplicate and triplicate measurements of the fragment shown as subsequent grey circles. Error bars are the internal precision (2SE) of solution measurements and do not reflect external precision (repeatability). The uncertainty bounds about the averages of the solution data are 2SD of the set of measurements.

Figure 7

Comparison of the accuracy of $^{87}Sr/^{86}Sr$ measurements for glass reference materials with ^{87}Rb interference corrections calculated using (A) βRb=βSr, or (B) an externally calibrated offset between βRb and βSr. The elemental Rb/Sr of the glass reference materials increases to the right. All $^{87}Sr/^{86}Sr$ values are normalised to BHVO-2G and are corrected for Kr, Rb, CaCa/CaAr, and REE^{2+} interferences. $\Delta^{87}Sr/^{86}Sr$ is the deviation in ppm of the measured isotope ratio from the recommended value. Individual vertical bars show the $\Delta^{87}Sr/^{86}Sr$ ± 2SE (propagated, ppm) for individual measurements with the mean deviation (± 2SD) shown as the grey horizontal bars and labelled above each set of measurements. Calculating the βRb-

βSr offset produces accurate results for reference glasses with Rb/Sr <0.30 (equivalent to the T1-G reference glass); above this value, the error in $^{87}Sr/^{86}Sr$ generally increases with increasing Rb/Sr. Note that the residual bias in the $^{87}Sr/^{86}Sr$ measurements of BCR-2G in Figure 7B is likely due to normalisation of the interference-corrected $^{87}Sr/^{86}Sr$ to BHVO-2G; the non-normalized values are centered approximately around 0 bias ($^{87}Sr/^{86}Sr$ of 6 ± 39 ppm).

Figure 8

Impact of different combinations of molecular interference corrections on the accuracy and precision of $^{87}Sr/^{86}Sr$ measurements for our reference plagioclase standards (A) and reference glasses (B). Each panel shows a single set of analyses (i.e. the same integration intervals) of three different reference materials subject to Kr baseline subtraction, Rb peak-stripping, and calculating the offset between βSr and βRb using BCR-2G as a bracketing standard and various combinations of molecular and doubly charged interference corrections. For example, the leftmost sets of analyses in each panel have only been corrected for Rb and Kr, whereas the rightmost sets show the same set of analyses but also corrected for CaCa/CaAr + REE interferences. $\Delta^{87}Sr/^{86}Sr$ is the deviation of the measured $^{87}Sr/^{86}Sr$ from the recommended value in ppm. Individual bars show the deviation and ± 2SE (internal) for individual measurements. The weighted mean and ± 2SD are shown as coloured horizontal bars and stated above each set of analyses. Thick grey horizontal bars encompass ± 2SD of the recommended value for each reference material. Panel (C) plots the error in $^{87}Sr/^{86}Sr$ as a function of the (Er+Yb)/Sr content of four low Rb/Sr reference glasses prior to correction for REE^{2+} interferences and normalisation to a primary standard. Note the positive correlation between error in $^{87}Sr/^{86}Sr$ and increasing (Er+Yb)/Sr.

Figure 9

Comparison of simulated interferences on $^{84}Sr/^{86}Sr$ and $^{87}Sr/^{86}Sr$ for a hypothetical measurement of a sample with $^{87}Sr/^{86}Sr = 0.710000$ and 0.5 V signal for ^{86}Sr. Note the differences in scale for $^{84}Sr/^{86}Sr$ and $^{87}Sr/^{86}Sr$ measurements, which indicate that the positive errors in $^{84}Sr/^{86}Sr$ (top, parts per ten thousand) due to the various interferences are up to 2 orders of magnitude larger than the corresponding error in $^{87}Sr/^{86}Sr$ (bottom, parts per million).

Figure 10

Relationship between spot/raster size, Sr content, and measurement precision in plagioclase. (A) Precision of $^{87}Sr/^{86}Sr$ measurements (2SE, internal) of plagioclase with varying Sr concentrations analysed with different spot sizes during this study. Note that the Sr concentrations were measured by LA-MC-ICP-MS and calibrated to BCR-2G so may underestimate the actual concentrations. Inset shows same data but plotted as a function of the signal on ^{88}Sr (V). All rasters were 200 μm in length and performed with a scan speed of 2 μm/s, using a 50 μm or 100 μm diameter beam. Dashed horizontal line shows a 100 ppm precision threshold. (B) Histogram of Sr contents of igneous plagioclase classified by host rock composition (Felsic = SiO_2 > 60%, Intermediate = SiO_2 50–60%, Mafic= SiO_2 <50%). (C) kernel density estimate of plagioclase XAn (%) vs. Sr (ppm). Data in panels B and C are from the GEOROC database (http://georoc.mpch-mainz.gwdg.de/georoc/) and the two dashed vertical lines in each panel show the approximate Sr content of plagioclase required to achieve ~100 ppm 2 SE precision with spot sizes of 100 μm and 64 μm for static spot analyses. Note that for a given Sr concentration, raster analysis may be used to resolve plagioclase zones too small for spot analysis at the same spot size.

Figure 11

Application of the LA-MC-ICP-MS Sr isotope measurement protocols outlined in this study to plagioclase and groundmass from Merapi Volcano, Indonesia. (A) X-ray fluorescence Ca map of a thin section of andesite from the 2010 eruption. Groundmass is purple, zoned plagioclase grains are orange-red, clinopyroxene grains are yellow-white. (B) Location of Sr isotope measurement spots and rasters for plagioclase and groundmass overlain on greyscale Ca map. Panels (C) and (D) show back scatter electron (BSE) images of two representative plagioclase grains. Panels (E) and (F) show schematic maps of the two representative plagioclase crystals and the location of LA-MC-ICP-MS rasters and microprobe spots. Panels (G) and (H) summarise the core-to-rim Sr isotope compositions colour-coded by XAn of each compositional domain as determined by electron microprobe analyses (panels I and J). Panel (K) compares the new results from the 2010 Merapi eruption to the micro-milled + TIMS Sr isotope measurements from the 1998 Merapi eruption (Chadwick et al., 2007). The white vertical bars on the left show the measured $^{87}Sr/^{86}Sr$ ± 2SE from 100 μm spot analyses of individual plagioclase crystals (locations in panel B), the grey horizontal fields show the mean ± 2SD $^{87}Sr/^{86}Sr$ of groundmass (this study) and TIMS wholerock $^{87}Sr/^{86}Sr$ data (Handley

et al., 2018), in excellent agreement with each other. The coloured symbols to the right show the micromilled + TIMS results from Chadwick et al. (2007). Panels (L) and (M) show petrogenetic models accounting for the Sr isotope systematics of compositionally zoned plagioclase crystals from the 1998 and 2010 Merapi eruptions.

Fig. 1

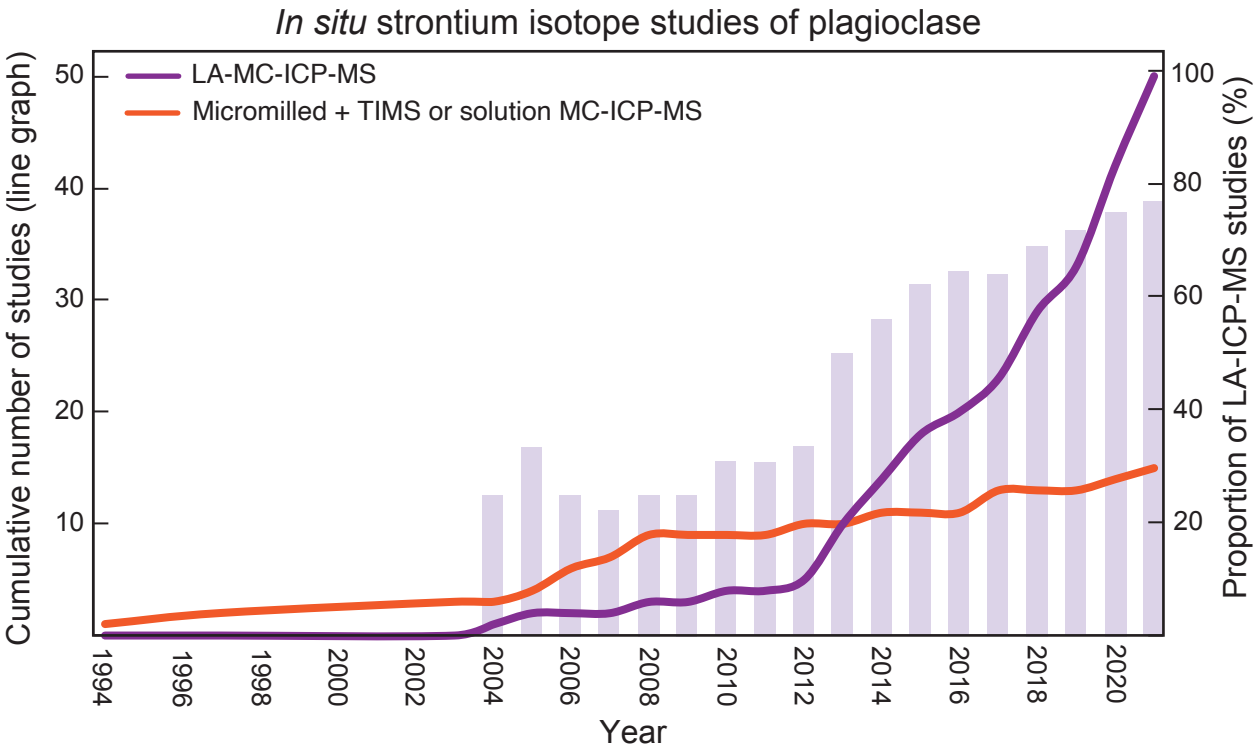
In situ strontium isotope studies of plagioclase
LA-MC-ICP-MS
Micromilled + TIMS or solution MC-ICP-MS
Cumulative number of studies (line graph)
Proportion of LA-ICP-MS studies (%)
Year
50
40
30
20
10
100
80
60
40
20
1994
1996
1998
2000
2002
2004
2006
2008
2010
2012
2014
2016
2018
2020

Fig. 2

Secondary standards

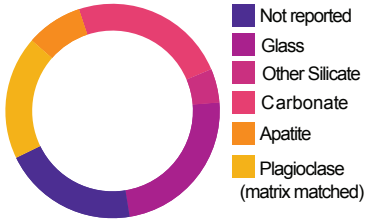

Stable isotope ratios

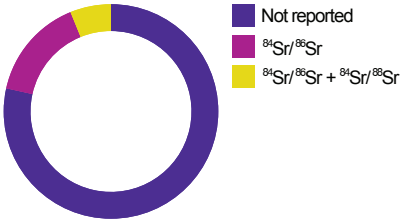

Doubly charged and molecular interefence corrections

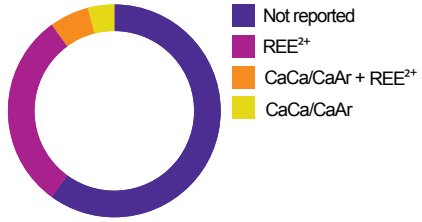

Fig. 3

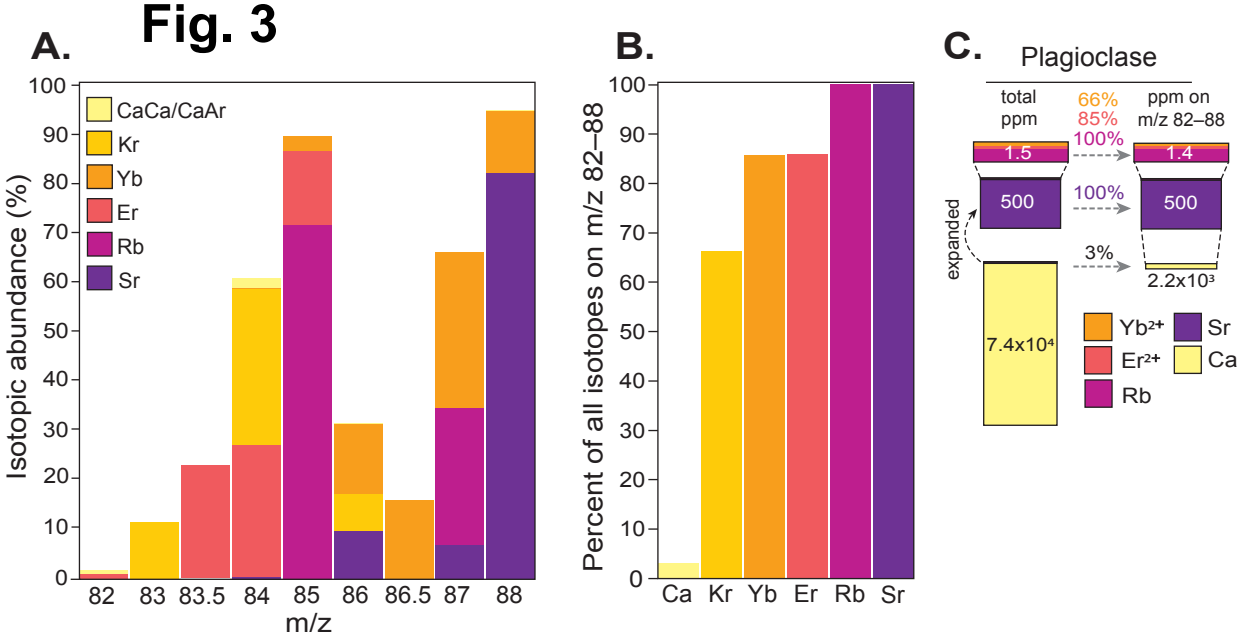
A.
Isotopic abundance (%)
CaCa/CaAr
Kr
Yb
Er
Rb
Sr
m/z
B.
Percent of all isotopes on m/z 82–88
Ca
Kr
Yb
Er
Rb
Sr
C.
Plagioclase
total ppm
66%
85%
100%
ppm on m/z 82–88
1.5
1.4
500
100%
500
expanded
3%
2.2x10³
7.4x10⁴
Yb²⁺
Sr
Er²⁺
Ca
Rb

Fig. 4

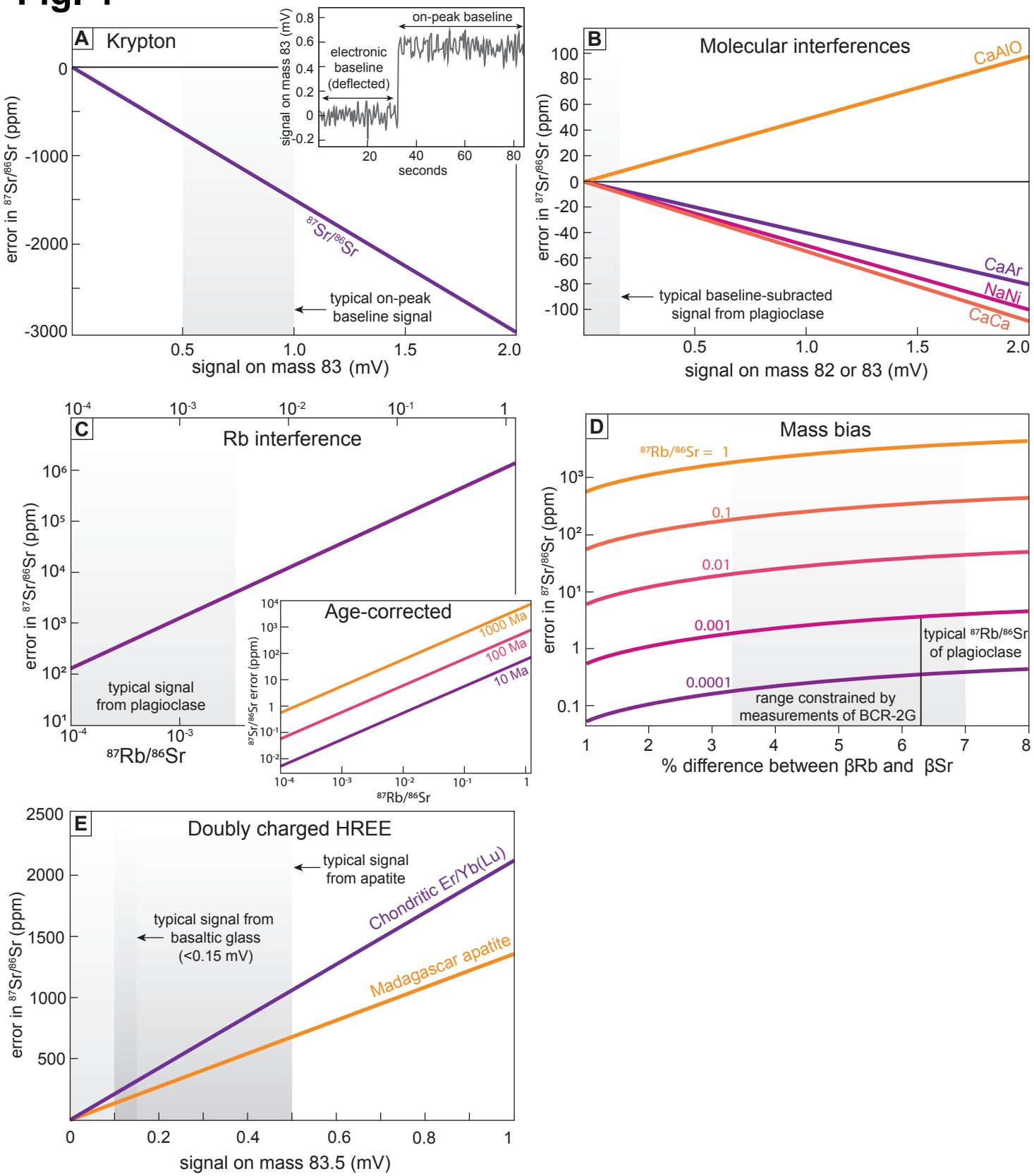
A
Krypton
error in $^{87}Sr/^{86}Sr$ (ppm)
signal on mass 83 (mV)
on-peak baseline
electronic baseline (deflected)
seconds
$^{87}Sr/^{86}Sr$
typical on-peak baseline signal
signal on mass 83 (mV)
B
Molecular interferences
CaAlO
CaAr
NaNi
CaCa
typical baseline-subracted signal from plagioclase
signal on mass 82 or 83 (mV)
C
Rb interference
typical signal from plagioclase
$^{87}Rb/^{86}Sr$
Age-corrected
1000 Ma
100 Ma
10 Ma
D
Mass bias
$^{87}Rb/^{86}Sr$ = 1
0.1
0.01
0.001
0.0001
typical $^{87}Rb/^{86}Sr$ of plagioclase
range constrained by measurements of BCR-2G
% difference between βRb and βSr
E
Doubly charged HREE
typical signal from apatite
typical signal from basaltic glass (<0.15 mV)
Chondritic Er/Yb(Lu)
Madagascar apatite
signal on mass 83.5 (mV)

Fig. 5

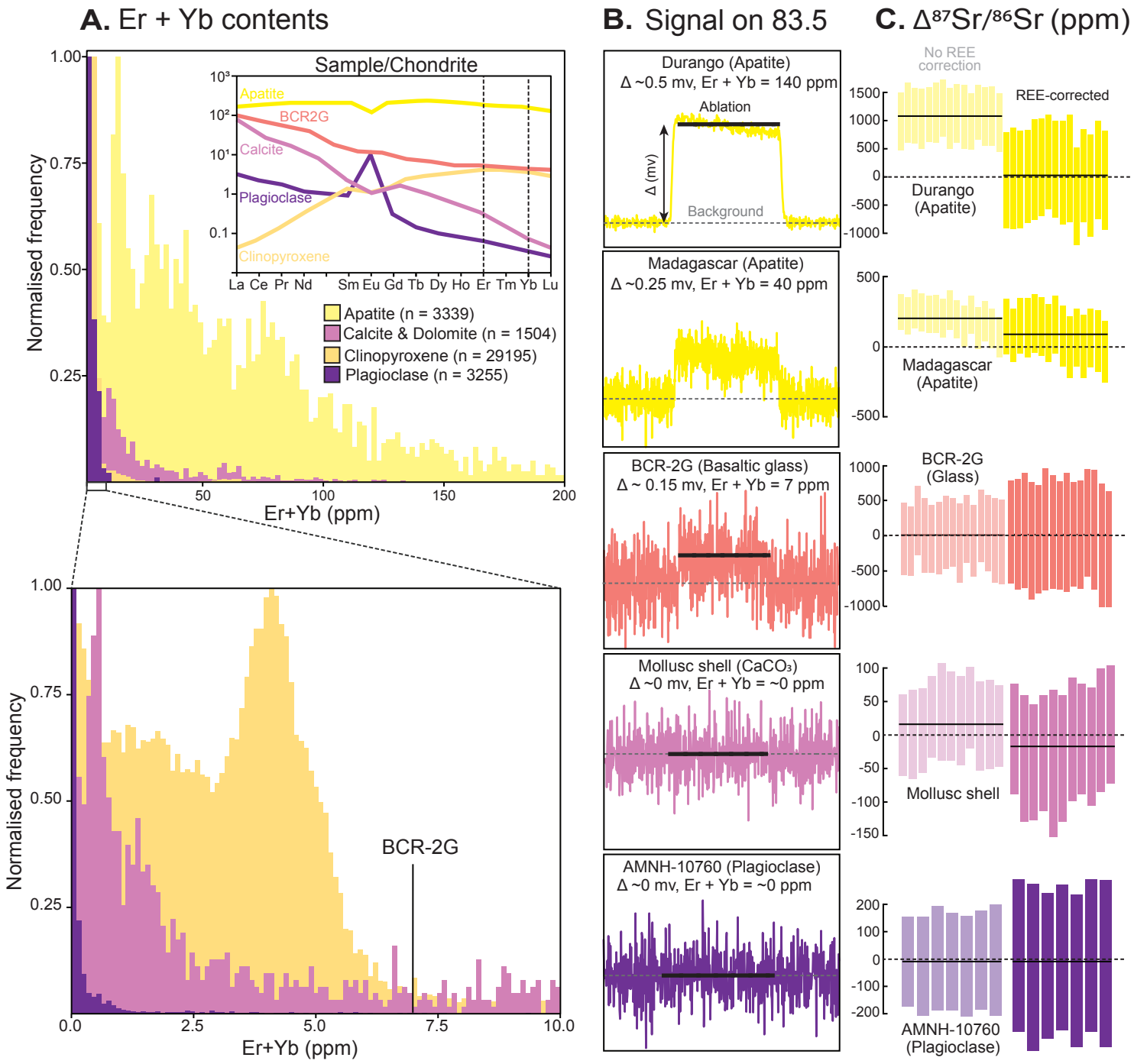
A. Er + Yb contents
B. Signal on 83.5
C. Δ87Sr/86Sr (ppm)
Sample/Chondrite
Apatite
BCR2G
Calcite
Plagioclase
Clinopyroxene
La Ce Pr Nd Sm Eu Gd Tb Dy Ho Er Tm Yb Lu
Apatite (n = 3339)
Calcite & Dolomite (n = 1504)
Clinopyroxene (n = 29195)
Plagioclase (n = 3255)
Normalised frequency
Er+Yb (ppm)
BCR-2G
Durango (Apatite)
Δ ~0.5 mv, Er + Yb = 140 ppm
Ablation
Δ (mv)
Background
Madagascar (Apatite)
Δ ~0.25 mv, Er + Yb = 40 ppm
BCR-2G (Basaltic glass)
Δ ~ 0.15 mv, Er + Yb = 7 ppm
Mollusc shell (CaCO3)
Δ ~0 mv, Er + Yb = ~0 ppm
AMNH-10760 (Plagioclase)
Δ ~0 mv, Er + Yb = ~0 ppm
No REE correction
REE-corrected
Durango (Apatite)
Madagascar (Apatite)
BCR-2G (Glass)
Mollusc shell
AMNH-10760 (Plagioclase)

Fig. 6

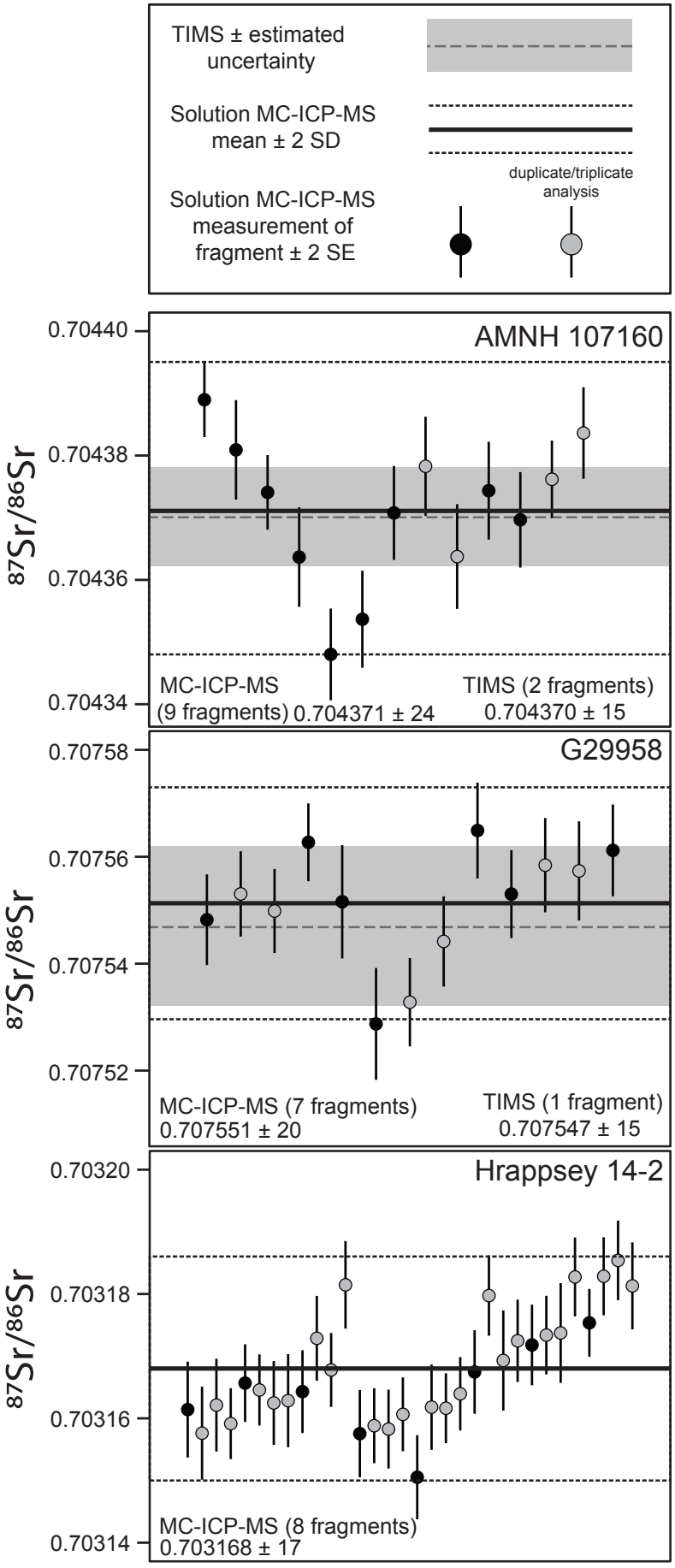
TIMS ± estimated uncertainty
Solution MC-ICP-MS mean ± 2 SD
duplicate/triplicate analysis
Solution MC-ICP-MS measurement of fragment ± 2 SE
AMNH 107160
0.70440
0.70438
0.70436
0.70434
87Sr/86Sr
MC-ICP-MS (9 fragments) 0.704371 ± 24
TIMS (2 fragments) 0.704370 ± 15
G29958
0.70758
0.70756
0.70754
0.70752
87Sr/86Sr
MC-ICP-MS (7 fragments) 0.707551 ± 20
TIMS (1 fragment) 0.707547 ± 15
Hrappsey 14-2
0.70320
0.70318
0.70316
0.70314
87Sr/86Sr
MC-ICP-MS (8 fragments) 0.703168 ± 17

Fig. 7

Sample	BIR-1G	GOR128	KL2	StHs6/80	BCR-2G	T1	GSD1	ATHO
Rb/Sr	0.002	0.014	0.024	0.064	0.137	0.281	0.538	0.694
Sr (ppm)	108.6	30	356	482	399.2	284	69.4	94.1

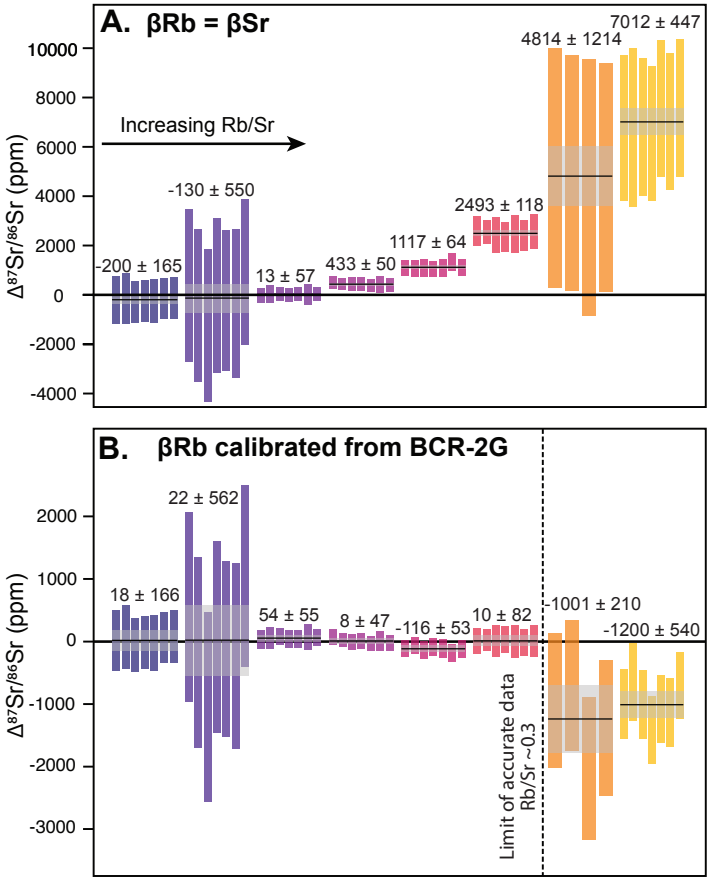

Fig. 8

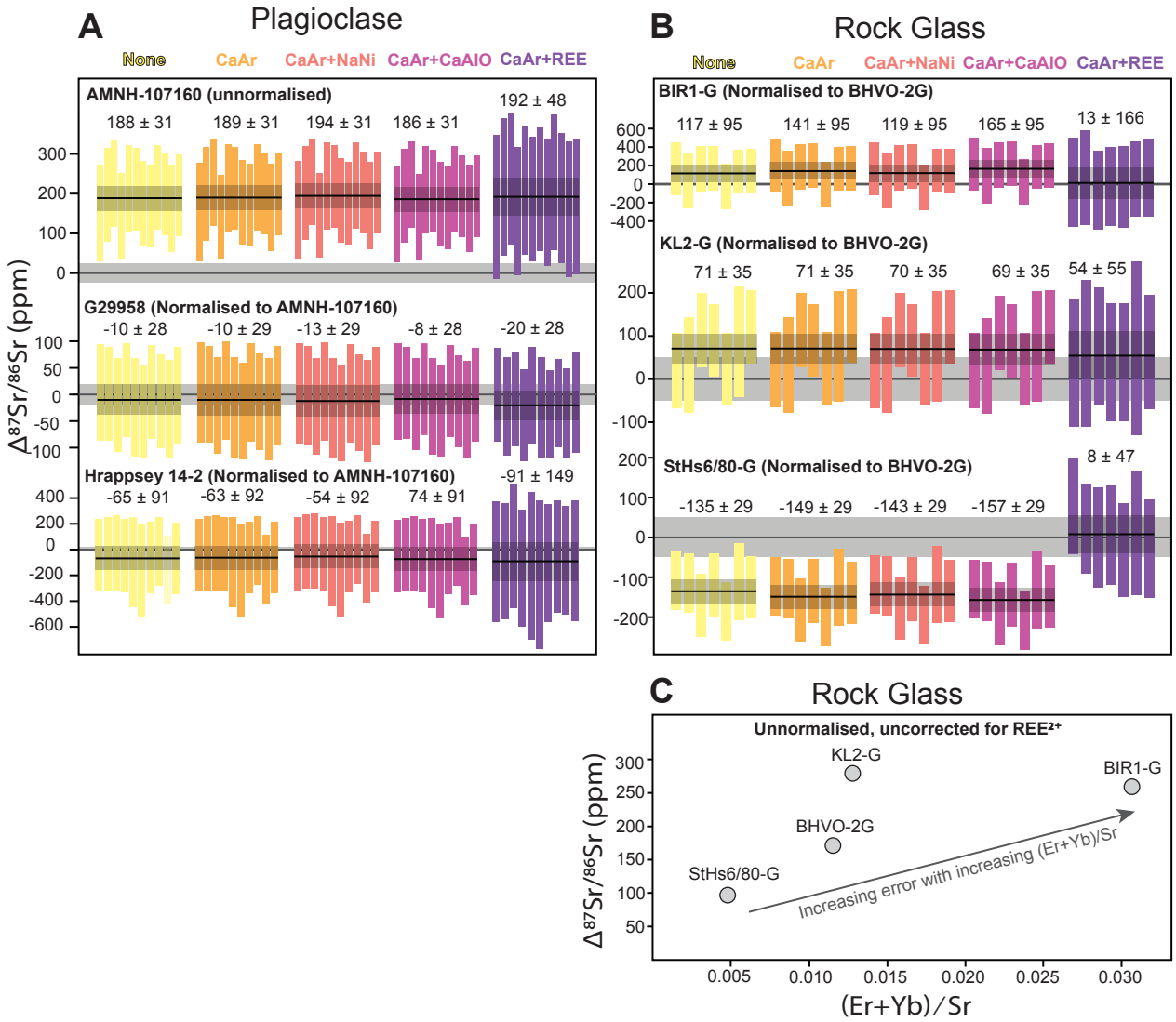
A
Plagioclase
None
CaAr
CaAr+NaNi
CaAr+CaAlO
CaAr+REE
AMNH-107160 (unnormalised)
188 ± 31
189 ± 31
194 ± 31
186 ± 31
192 ± 48
G29958 (Normalised to AMNH-107160)
-10 ± 28
-10 ± 29
-13 ± 29
-8 ± 28
-20 ± 28
Hrappsey 14-2 (Normalised to AMNH-107160)
-65 ± 91
-63 ± 92
-54 ± 92
74 ± 91
-91 ± 149
Δ87Sr/86Sr (ppm)
B
Rock Glass
BIR1-G (Normalised to BHVO-2G)
117 ± 95
141 ± 95
119 ± 95
165 ± 95
13 ± 166
KL2-G (Normalised to BHVO-2G)
71 ± 35
71 ± 35
70 ± 35
69 ± 35
54 ± 55
StHs6/80-G (Normalised to BHVO-2G)
-135 ± 29
-149 ± 29
-143 ± 29
-157 ± 29
8 ± 47
C
Rock Glass
Unnormalised, uncorrected for REE2+
KL2-G
BIR1-G
BHVO-2G
StHs6/80-G
Increasing error with increasing (Er+Yb)/Sr
Δ87Sr/86Sr (ppm)
(Er+Yb)/Sr

Fig. 9

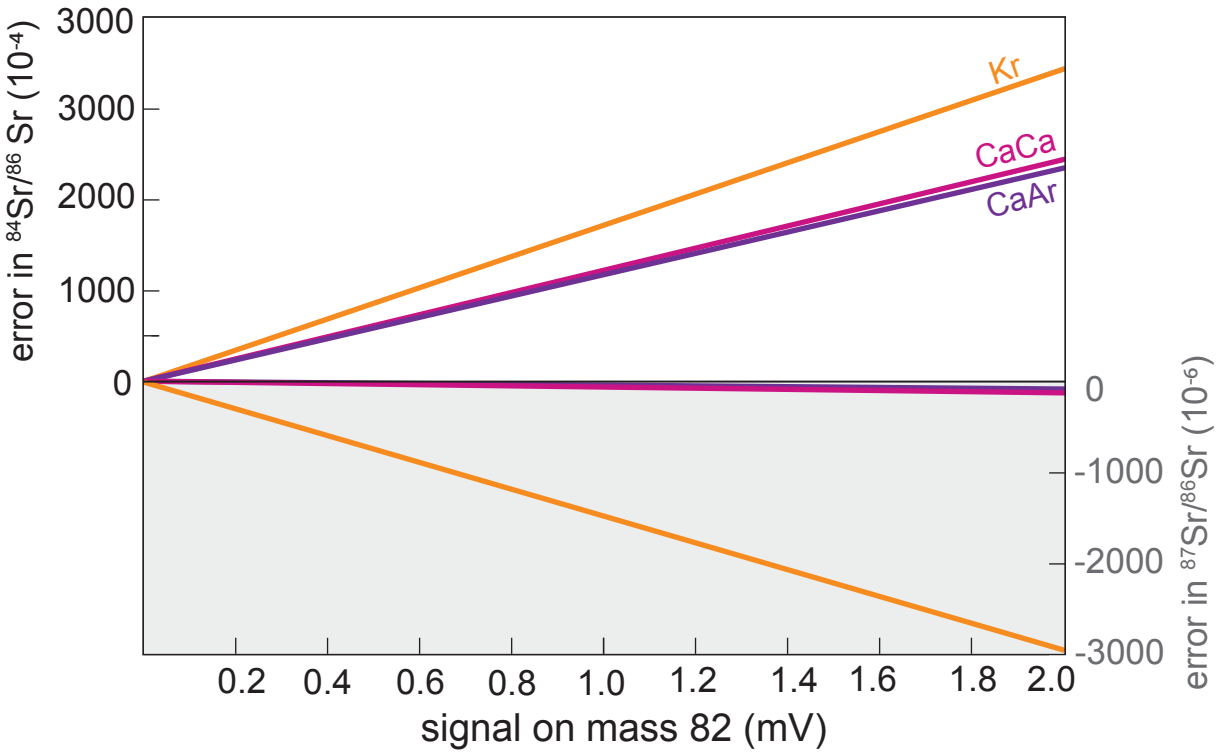
3000
3000
2000
1000
0
error in $^{84}Sr/^{86}Sr$ (10^{-4})
Kr
CaCa
CaAr
0
-1000
-2000
-3000
error in $^{87}Sr/^{86}Sr$ (10^{-6})
0.2
0.4
0.6
0.8
1.0
1.2
1.4
1.6
1.8
2.0
signal on mass 82 (mV)

Fig. 10

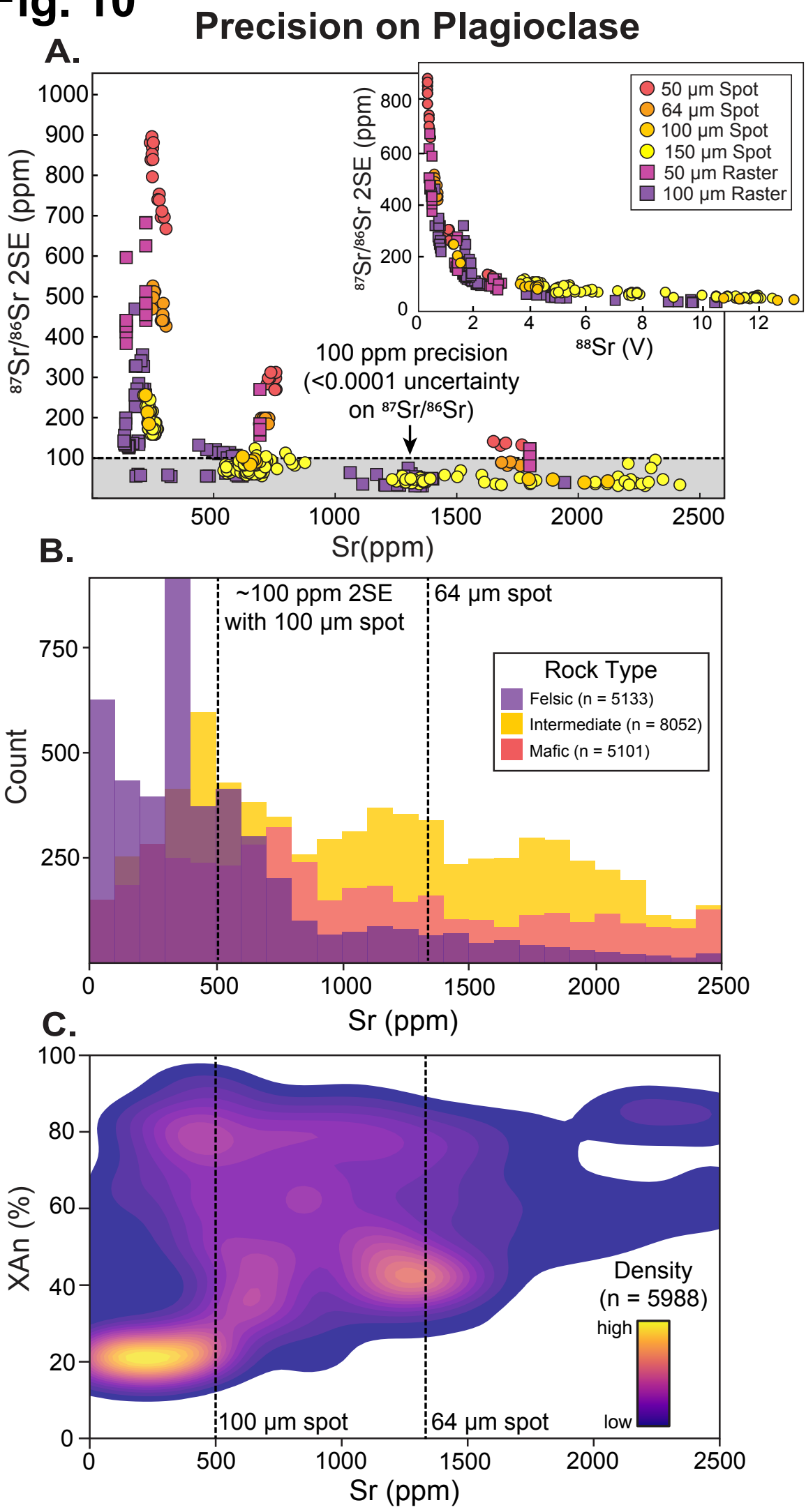
Precision on Plagioclase
A.
$^{87}Sr/^{86}Sr$ 2SE (ppm)
Sr(ppm)
50 µm Spot
64 µm Spot
100 µm Spot
150 µm Spot
50 µm Raster
100 µm Raster
^{88}Sr (V)
100 ppm precision
(<0.0001 uncertainty
on $^{87}Sr/^{86}Sr$)
B.
Count
Sr (ppm)
~100 ppm 2SE
with 100 µm spot
64 µm spot
Rock Type
Felsic (n = 5133)
Intermediate (n = 8052)
Mafic (n = 5101)
C.
XAn (%)
Sr (ppm)
100 µm spot
64 µm spot
Density
(n = 5988)
high
low

Fig. 11 Merapi Andesite

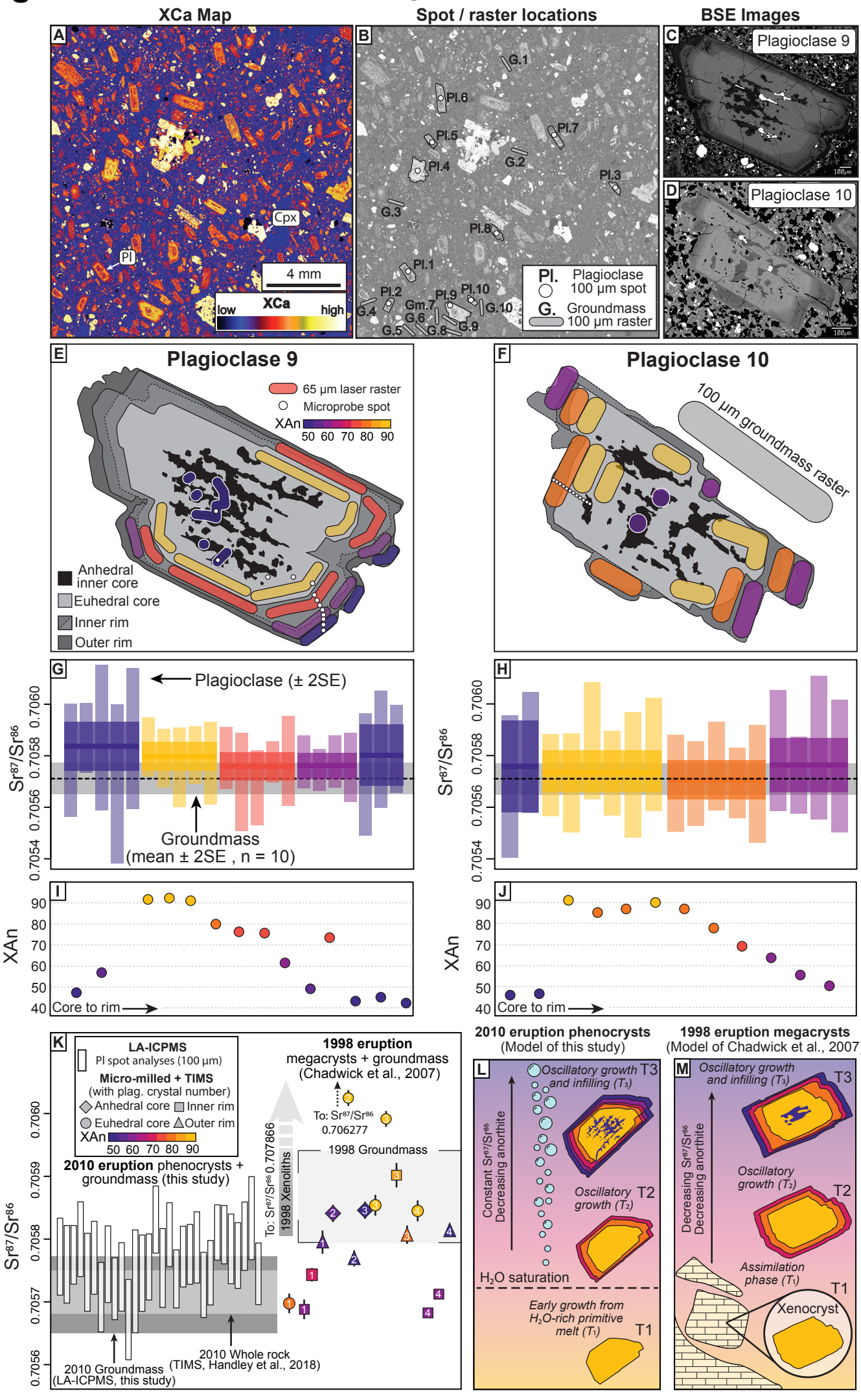

SUPPLEMENTARY MATERIAL CAPTIONS

Supplementary File 1

Table summarising instrumental set up and analytical conditions

Supplementary File 2

Table of LA-MC-ICP-MS results

Supplementary File 3

Solution ICP-MS and TIMS results

Supplementary File 4

Iolite DRS

Supplementary File 5

Explanation of DRS

Supplementary Figure 1

Plot of baseline subtract signals on masses 83 and 82 and the 82/83 ratio for a set of analyses of three different plagioclase reference materials with differing anorthite contents. There is a subtle increase in signals on masses 82 and 83 with increasing anorthite content, consistent with an increasing contribution from CaCa/CaAr interferences. In contrast, there is no correlation between 82/83 and anorthite content, suggesting contribution from CaAlO or NaNi is not dependent on the composition of plagioclase.

Supplementary Figure 2

Effect of downhole fractionation on $^{84}Sr/^{86}Sr$ measurements. (A) Shows individual 45 second analyses of three reference plagioclases. The individual points show measured ratios ± 2SE (internal) for 5 second intervals that track the measured ratio as a function increasing pit depth during analysis. Coloured horizontal bars encompassing the weighted mean value and 2SE (internal) of the entire 45 second analysis. Dashed horizontal lines show the recommended $^{84}Sr/^{86}Sr$ ratio (0.0565). In theory, the 50 μm spot analyses should be the most impacted by downhole fractionation effects (greatest pit depth-to-width ratio), whereas the

100 μm raster should be least impacted. However, we observe no significant downhole fractionation effects on the $^{84}Sr/^{86}Sr$ ratio for any of the tests.

Supplementary Figure 3

Impact of different combinations of molecular interference corrections on the accuracy and precision of $^{84}Sr/^{86}Sr$ for plagioclase (left panels) and rock glass reference materials (right panels). Each panel shows a single set of analyses (i.e. the same integration intervals) of three different reference materials subject to various interference corrections. For example, the leftmost sets of analyses in each panel have had no interference corrections applied, whereas the rightmost sets show the same set of analyses but corrected for CaCa/CaAr + REE interferences. $\Delta^{84}Sr/^{86}Sr$ is the deviation of the measured isotope ratio from the recommended value. Individual bars show the deviation and ± 2SE (internal) for individual measurements. The weighted mean and ± 2SD are shown as coloured horizontal bars and stated above each set of analyses.

Supplementary Figure 1

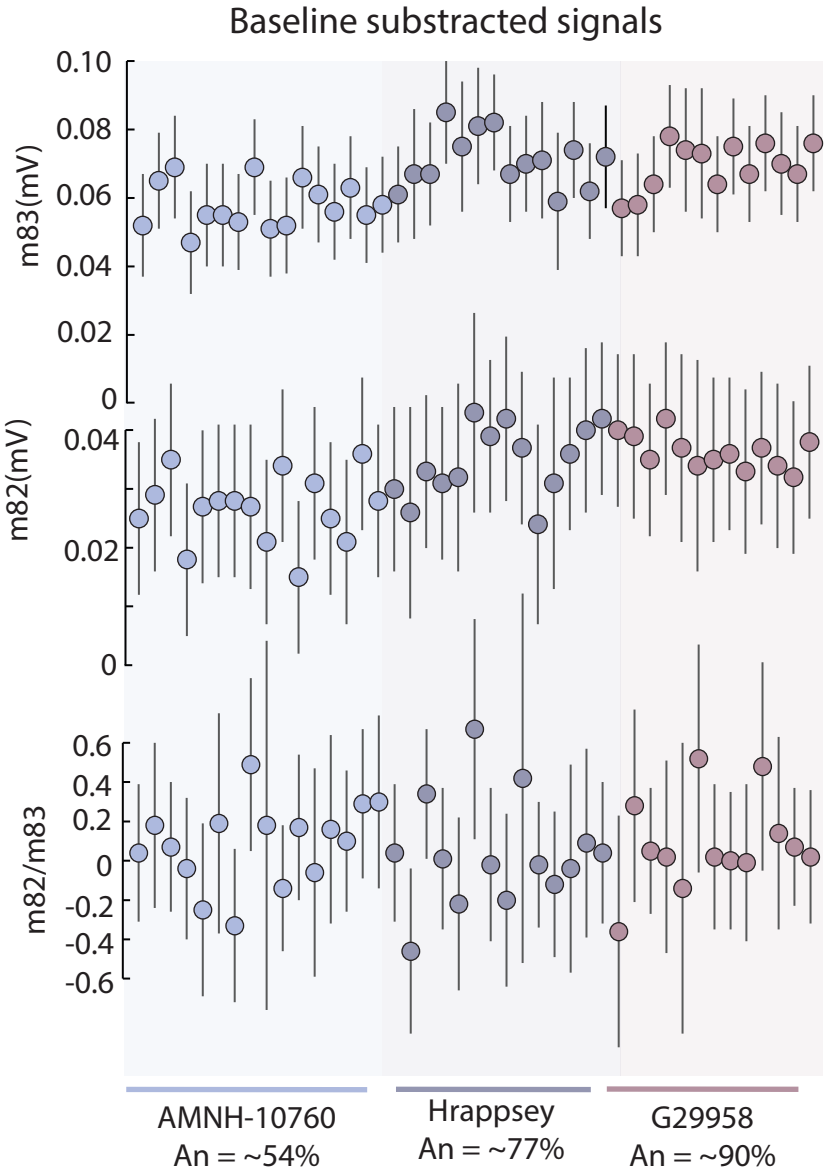

Supplementary Figure 2

A. Individual analyses

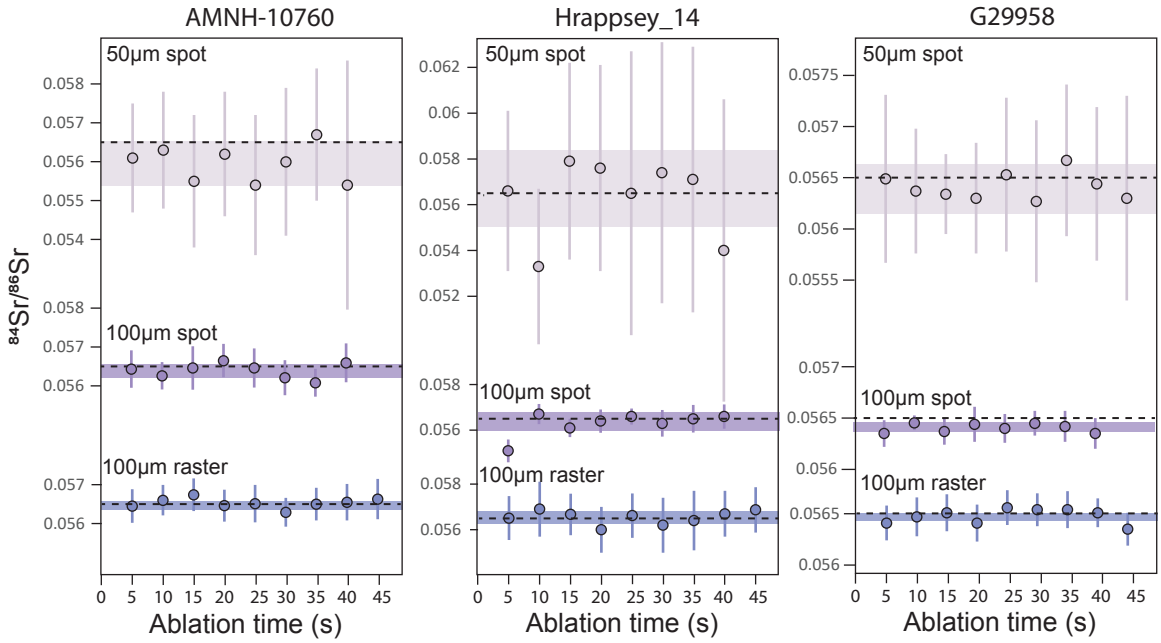

Supplementary Figure 3

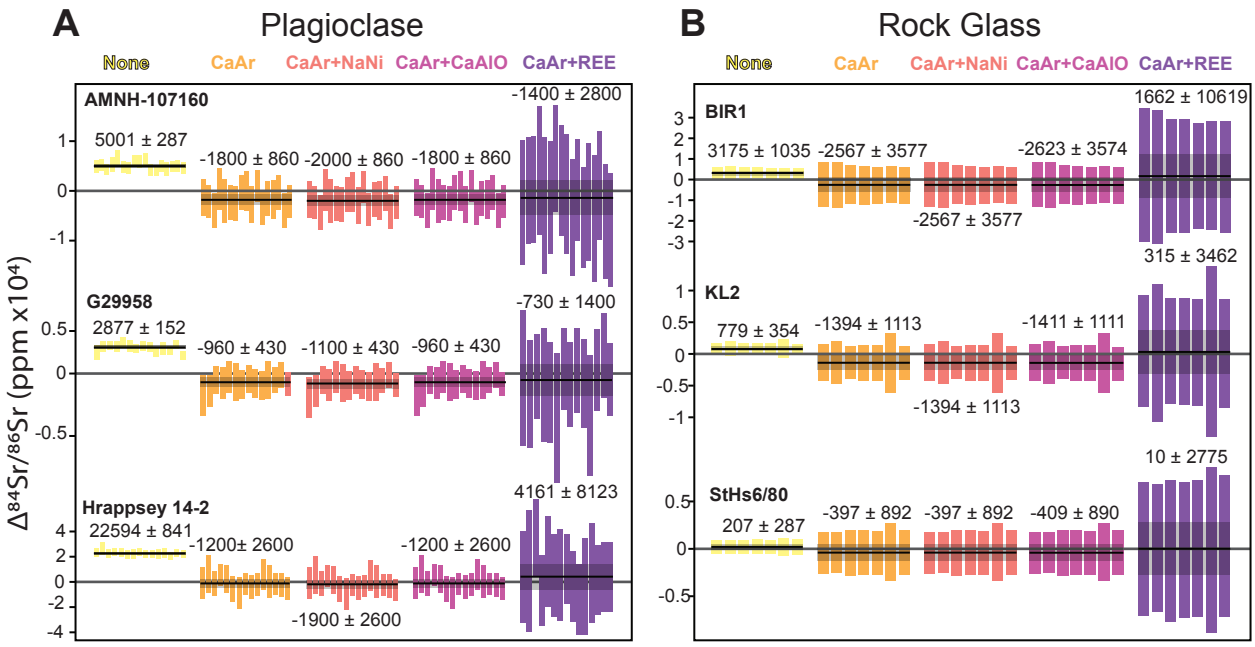

Supplementary File 3: Iolite DRS

Please note that the DRS will continue to be updated and developed. The most recent version of the DRS can be found at: https://github.com/iolite-LA-ICP-MS/iolite4-python-examples/blob/master/drs/Sr_isotopes_Universal.py

***Note the URL in the PDF version of this file may contain a space at the end of line one (after 'python-'). Please remove this when copying into a web browser.**

Explanation of Sr Isotopes Universal DRS

Please note that the DRS will continue to be developed and updated. The most recent version of the DRS and these expanatory notes can be found at: https://github.com/iolite-LA-ICP-MS/iolite4-python-examples/blob/master/drs/Sr_isotopes_Universal.py

The "Sr Isotopes Universal" DRS provides a number of user-selectable options for reducing Sr isotope data measured by LA-MC-ICP-MS. Since the first Sr isotope measurements by LA-MC-ICP-MS (to our knowledge, Christensen et al., 1995), there have been a number of articles that have outlined and evaluated various potential sources of bias (predominately the multitude of interferences on all Sr isotope masses) in the measurements and proposed various corrections for these sources of bias (e.g., Woodhead et al., 2004; Vroon et al., 2008; Kimura et al., 2014; Müller & Anczkiewicz, 2016). All of these employ "peak-stripping" of interferences (monitoring a nominally interference-free isotope of the interfering element and using canonical isotopic abundances to subtract its interferences on the Sr isotopes of interest) at some point in the correction scheme. Many different atomic, molecular, and doubly charged interferences have been considered (most of which are covered in Vroon et al., 2008, Kimura et al., 2014, and Müller & Anczkiewicz, 2016), and they are matrix-dependent. For example, doubly charged REE ("REE^{2+}") may yield significant interferences in apatite but be negligible in plagioclase and carbonates. The Sr Isotopes Universal DRS allows users to choose different combinations of interferences to subtract from their data, depending on the expected and/or observed interferences for their samples. There are also several other corrections that can be performed. Users can choose to subtract different combinations of REE^{2+}, CaAr-CaCa, NaNi-CaAlO inteferences; calculate an adjusted Rb mass-bias factor to improved the accuracy of the ^{87}Rb interference correction; correct for Rb-Sr elemental fractionation, which may affect age-correction; and/or correct for residual biases in $^{87}Sr/^{86}Sr$ following other corrections, which could be attributed to uncorrected $^{87}(CaPO)$. This document describes the options in the DRS and the results calculated based on the selected options.

Krypton and Rb interferences are always applied in the DRS. The former is corrected thorugh on-peak baseline (which can be fit by one of Iolite's many spline types) subtraction (see Kimura et al., 2014 for an alternative approach) and the latter from monitoring ^{85}Rb and peak-stripping. Users can additionally choose to subtract REE^{2+}, CaAr-CaCa, NaNi-CaAlO inteferences. The corrections can be selectively applied by selecting or deselecting check-boxes in the DRS settings. If all these (or some combination of these) interferences are assumed to be present and chosen to be subtracted, they are necessarily subtracted that order. For example, doubly charged Er (± Dy) should be subtracted from masses 83 and 82 (in addition to the Sr masses) before carrying out a CaAr-CaCa correction using 83 or 82 as a monitor mass. Nominal mass-bias factors based on $^{88}Sr/^{86}Sr$ are applied to these interferences. For each step in the correction (e.g., after $^{172}Yb^{2+}$, and $^{176}Yb^{2+}$ and $^{176}Lu^{2+}$ have been subtracted from 86 and 88, respectively), an updated nominal $^{88}Sr/^{86}Sr$ mass-bias factor is calculated and applied to subsequent corrections. The CaAr-CaCa interferences can be monitored on either mass 82 or 83 (there are isotopologues of these molecules with both these masses). Notice that CaAr and CaCa are considered together. This is because both molecules have isotopologues with mass 82 and 83. Therefore, the user must assume and enter a proportion of the signal on mass 82-83 attributable to CaAr and CaCa in order to subtract these from the Sr masses based on canonical isopologue proportions. In theory, the 83/82 signal ratio could be used to calculate the proportion, but this ratio is likely very imprecise due to low signal intensities. The same combined subtraction applies to NaNi and CaAlO, although these have significant isotopologues only of mass 83 and not 82. Several other settings relevant to these optional corrections are described in the setting-by-setting descriptions below.

Interferences of ^{87}Rb on ^{87}Sr are significant, even in matrices with low to moderate Rb/Sr (e.g., carbonates and plagioclase). Because Rb has only one nominally interference-free isotope (^{85}Rb), a mass-bias factor cannot be directly determined for Rb. It is common practice to apply the Sr mass-bias factor based on ^{88}Sr/^{86}Sr ("βSr") to Rb (and other interference corrections). However, this has been demonstrated to fail at moderate to high Rb/Sr, with a pseudo-linear relationship between ^{87}Sr/^{86}Sr bias and Rb/Sr after ^{87}Rb subtraction (e.g., Jackson & Hart, 2006), which can be attributed to differences in the magnitude of Sr and Rb mass bias. Previous studies (e.g., Jackson & Hart; Zhang et al., 2018) have used glass standards with moderately high Rb/Sr or Rb-doped Sr isotope solutions to calibrate βRb or an adjusted ^{85}Rb/^{87}Rb (which are equivalent in effect on the correction). This DRS allows the user to calculate βRb using measurements of a reference material with moderately high Rb/Sr and known ^{87}Sr/^{86}Sr (BCR-2G used by default) and solving for βRb in the equation below. Obviously, measurements of the reference glass must be included in the sequence of analyses that are being reduced.

$$^{87}Sr/^{86}Sr_{ref} = [\ ^{87}(Sr,Rb) - ^{85}Rb * (^{87}Rb/^{85}Rb_{ref}) * (mass^{87}Rb/mass^{85}Rb)^{(\beta Rb)}] * (mass^{87}Sr/mass^{86}Sr)^{(\beta Sr)} * (1/^{86}Sr_{cor})$$

where:
$^{87}Sr/^{86}Sr_{ref}$ *is the Sr isotope ratio of the bracketing standard*
$^{87}(Sr,Rb)$ *is the signal on mass 87 with all other interferences subtracted*
^{85}Rb *is the raw signal on mass 85*
$^{87}Rb/^{85}Rb$ *is a canonical natural Rb isotope ratio*
$^{86}Sr_{cor}$ *is the interference-corrected* ^{86}Sr *signal*

Significant elemental fractionation between Sr and Rb has been observed to occur in LA-MC-ICP-MS measurements (Zhang et al., 2018). In samples that are old and/or have high Rb/Sr, accurately determining the ^{87}Rb/^{86}Sr of the sample is critical to accurate age-correction (i.e., calculating the ^{87}Sr/^{86}Sr at the time of isotopic equilibrium—e.g., crystallization—of the sample). Users can use measurements of a reference material with known Rb/Sr (BCR-2G by default) to calculate an elemental-fractionation-corrected ^{87}Rb/^{86}Sr to use in online or offline age-correction. Note that various mineral matrices will not necessarily yield the same Rb-Sr fractionation as the calibration reference material, but the correction utilizes this assumption. Also note that—currently—no downhole-correction for the Rb/Sr is performed by the DRS.

Finally, the DRS allows for the correction of residual bias in ^{87}Sr/^{86}Sr ratios following all other interference corrections and direct normalization to a primary reference material. This may appear to be "fudging" the data, but the approach may be practical in the case of interferences that cannot be independently monitored and subtracted from the Sr masses. A relevant example is the interference of ^{87}(CaPO)—the major isotopologue of a molecule which may obviously be present in apatite analyses and which does not have isotopologues that are practically measurable on other detectors in the array. Therefore, there is no practical way to correct for this interference aside from an empirical secondary correction following other peak-stripping corrections. The correction is done by fitting a linear or exponential model to the data in ^{87}Sr/^{86}Sr bias vs Sr signal space, assuming that the magnitude of an interference from a stoichiometric component—like CaPO in apatite—is inversely proportional to Sr signal (i.e., 1/Sr signal if the CaPO signal is constant).

As a final and obvious note, the user of the DRS must use some intuition in deciding which corrections to apply to their data. Some of the interferences have only briefly been considered in the

literature (in-particular the NaNi-CaAlO interferences discussed in Kimura et al., 2014) and may not be relevant to any common matrices. Applying unnecessary corrections may increase measurement uncertainties (e.g., applying the REE^{2+} corrections if there is baseline signal on the half-masses) or *introduce* bias in the corrected $^{87}Sr/^{86}Sr$. The corrections that can be applied also depend on the masses measured on the particular detector array. At minimum, the DRS requires 88, 87, 86, 85, and 84 for the basic mass-bias and Rb-interference corrections (perhaps we will eventually remove 84 from this list). Other corrections rely on monitoring interferences on particular masses. If the relevant masses are not measured, the user will get an error message (e.g., if CaAr-CaCa correction is selected but there are no data for the monitor mass 82 or 83).

As a final, final note, this DRS (as is the case with most Iolite DRS) is a work in progress. It is likely that it will be changed (hopefully improved) in the future, perhaps with your input. We will try to accompany all updates with notes.

DRS Settings

Index channel: This is present in most Iolite DRS. I am not actually sure what it is used for. In this DRS, it is set to m88 (the most abundant Sr isotope) by default.

Reference material: Primary standard for final normalization of $^{87}Sr/^{86}Sr$ after all interference and mass-bias corrections have been done

Mask and related settings: Enables a signal-threshold criterion to be used for masking data in the Time Series window. To my knowledge, the mask doesn't exclude points from calculations for selections, but I may be wrong about this. This is also common to most Iolite DRS.

REE subtraction ?: If checked, REE^{2+} will be subtracted from masses 84, 85, 86, 87, and 88 (and 82 and 83 if those channels are present). The corrections rely on signals for the half-masses: 83.5, 86.5, 87.5, so these channels need to be present to carry out the calculations.

Dy/Er ratio (default is approximately chondritic): Doubly charged Er interferes on mass 83, and doubly charged Er and Dy interfere on mass 82, the latter of which can be selectively used for subsequent correction of CaAr-CaCa. $Erbium^{2+}$ is monitored on "half-mass" 83.5 and can be subtracted from masses 82 and 83, but Dy^{2+} is not independently monitored on many faraday cup configurations. Therefore, a defined Dy/Er ratio is used to subtract Dy^{2+} from mass 82. The default (1.5) was very loosely chosen the ordinary chondrite composition of Nakamura (1974). This should be constrained for individual samples if the REE^{2+} interferences are significant.

Scale REE Beta (1 = BetaSr): The nominal $^{88}Sr/^{86}Sr$ mass-bias factor (I say "nominal" because it is calculated before all the interferences are subtracted) can be scaled if the user things the mass-bias factor for the REE is different. In theory, the REE mass-bias could be directly determined by monitoring $^{173}Yb^{2+}$ and $^{171}Yb^{2+}$, but this would likely be very imprecise for small signals on the half mass. If signals are small, the difference in mass-bias is likely to have a negligible effect anyway. The default (1) is that the REE mass-bias equals nominal Sr mass-bias.

CaAr-CaCa_subtraction?: If "yes", CaAr and/or CaCa interferences will be subtracted from all relevant channels. The corrections rely on signals for either 82 or 83 as a monitor mass, so one of these channels need to be present to carry out the calculations.

Use 83(CaAr,CaCa) as monitor? (uses 82 as default otherwise): If checked, the signal on mass 83 will be used as the monitor mass for the CaAr-CaCa peak-stripping. Otherwise (default), 82 will be used. If 83 is used, this assumes that the signal on mass 83 (the only potential monitor mass for NaNi-CaAlO) is due entirely to CaAr-CaCa, so a subsequent NaNi-CaAlO correction cannot be done.

Proportion CaAr (0 to 1): Because CaAr and CaCa are monitored on the same monitor mass (82 or 83), the signal on this mass may be due to a mixed contribution from each molecule. Therefore, a proportion of the monitor signal from each molecule needs to be assumed to subtract the interferences on the Sr masses using canonical abundances of the isotopologues of the different molecules. A value of 1 (default) assumes that 100% of the signal is due to CaAr. A value of 0 assumes that 100% of the signal is due to CaCa. If a value outside the range of 0 to 1 is entered, you will get an error message. Differences in assumed proportion of these molecules will have the largest effect on the subtractions from masses 85, 86, and 87 because CaCa has significant isotopologues on 85 and 87, whereas CaAr does not, and CaCa has a greater abundance of isotopologues 86 than CaAr. Whether differences in assumed proportions have a significant effect on most datasets is yet to be explored.

Scale CaAr-CaCa Beta (1 = BetaSr): The same as for the REE mass-bias scalar.

NaNi-CaAlO subtraction?: If "yes", NaNi and/or CaAlO interferences will be subtracted from all other signals.

Proportion NaNi (0 to 1): The same principle as for "Proportion CaAr". A value of 1 (default) assumes that 100% of the signal is due to NaNi. A value of 0 assumes that 100% of the signal is due to CaAlO. If a value outside the range of 0 to 1 is entered, you will get an error message. There are significantly different abundances of the isotopologues of these molecules on the Sr masses, but whether differences in assumed proportions have a significant effect on most datasets is yet to be explored.

Scale NaNi-CaAlO Beta (1 = BetaSr): The same as for the REE mass-bias scalar.

Rb Beta adjust?: Gives you the option to carry out the calculation of the Rb mass-bias factor based on a standard ("Reference material Rb beta"). Do not check this if you haven't measured a standard with moderately high Rb/Sr (e.g., BCR-2G) for this calculation.

Reference material Rb beta: Reference material used for calculating an adjusted Rb mass-bias factor using the equation outlined above. The calculation depends on the ^{85}Rb signal, among other things, and so it's important to have a reference material with relatively high Rb content. BCR-2G is the default and seems to work well.

Scale Rb beta (if Rb Beta adjust unchecked; 1 = BetaSr): If no moderately high Rb/Sr reference material is measured, a scaling factor can be applied to βSr to yield an adjusted βRb. However, instead of directly calculating βRb directly, you need to iteratively try different βSr scalars to

minimize the bias in $^{87}Sr/^{86}Sr$ for moderately high Rb/Sr reference materials. If "Rb Beta adjust?" is checked, this scalar will not be used.

Rb-Sr fractionation?: Gives you the option to normalize the measured (interference- and mass-bias-corrected) Rb/Sr to an external reference material. This may be important for age-correcting samples that are old and have relatively high Rb/Sr. Keep in mind that minerals and rock glasses may not yield the same Rb-Sr fractionation (i.e., because they are not matrix-matched), yet this correction (if using a rock glass as a reference material) relies on the assumption that they are. We assume that the correction will nonetheless improve the accuracy of the determined Rb/Sr, assuming that the significant interelement fractionation between Rb and Sr in the measurement (albeit tuning-condition-dependent; Zhang et al., 2018) is greater than that induced by matrix effects. This has not been tested though, due to a paucity of mineral standards with uniform, known Rb/Sr.

Reference material Rb/Sr fractionation: Reference material for correcting for Rb/Sr elemental fractionation in the measurement.

Scale Rb/Sr (if no Rb/Sr standard): If you haven't measured a standard with moderately high and well-characterized Rb/Sr, the measured Rb/Sr can be scaled by entering a value other than 1 here. However, if no reference materials with well-characterized Rb/Sr are measured, it will be impossible to evaluate the accuracy of the correction.

Age (Ma): The age of your sample in Ma for calculating age-corrected $^{87}Sr/^{86}Sr$ ($^{87}Sr/^{86}Sr_i$). The DRS uses the "final" $^{87}Rb/^{86}Sr$ (elemental-fractionation-corrected if selected) and the ^{87}Rb decay constant of Villa et al. (2015). Currently, the DRS uses the present-day $^{87}Sr/^{86}Sr$ after interference (including Rb with or without an adjusted βRb) but before the optional CaPO correction. We will soon fix this. Regardless, it is often more practical to do an age-correction offline on the Iolite output (therefore applying the age correction to the average final $^{87}Sr/^{86}Sr$ of the selections instead of point-by-point in Iolite), especially if you are measuring multiple samples with different ages.

CaPO Fit Eqn: The form of the function (linear or exponential decay) used to fit the data in $^{87}Sr/^{86}Sr$ bias vs Sr signal space for correction of residual $^{87}Sr/^{86}Sr$ bias after all other interference and mass-bias corrections. As the name implies, this may be relevant to apatite because $^{87}CaPO$ cannot not be independently peak-stripped. Because it is a stoichiometric component in apatite, one might expect a relationship between $^{87}Sr/^{86}Sr$ bias and Sr signal (or 1/Sr signal; proportional to CaPO/Sr signal).

RMs for CaPO correction: A dropdown that will populate with all reference materials from your session that have reference $^{87}Sr/^{86}Sr$. The reference materials used to establish the relationship (the model fit) between $^{87}Sr/^{86}Sr$ bias and Sr signal are chosen here. Keep in mind that if all reference materials from a session are used for the correction, they are all in a sense self-normalized, and there are not reference materials left to treat as quality-control or "secondary" standards. If applying this additional correction, it is probably good to measure as many reference materials (apatite in this case) as possible to define the fit as best as possible and to assure that it applies to a wide range of apatite.

CaPO Correction fit: Graph that shows the $^{87}Sr/^{86}Sr$ bias vs Sr signal for individual selections of the reference materials chosen above. Each dot of a particular color represents one selection of a particular reference material selection group.

Propagate Errors?: This is the same as other Iolite DRS. It calculates excess variance in selections of a reference material and propagates additional uncertainty into the measurement uncertainties. See the Iolite manual for more information.

DRS Outputs (Intermediate and Output Channels)

mXX.X_cps: Baseline-subtracted signals for each input channel.

Sr84,…Sr88, Rb85: Signals for the Sr and Rb isotopes following the all interference corrections.

Sr87_86_Corr: Interference- and mass-bias-corrected $^{87}Sr/^{86}Sr$ calculated by applying βSr to Rb but before final normalization of $^{87}Sr/^{86}Sr$ to a primary reference material. This result is included so the $^{87}Sr/^{86}Sr$ calculated with and without the adjusted βRb can be compared.

BetaSr: The final Sr mass-bias factor, calculated from "Sr88" and "Sr86" following all interference corrections. This is the mass-bias factor applied to the final $^{87}Sr/^{86}Sr$.

BetaRb: The Rb mass-bias factor, either directly calculated from a reference material if "Rb Beta adjust" is selected, scaled from βSr if a value other than 1 is entered for "Scale Rb Beta", or equal to βSr if "Rb Beta adjust" is not selected and the scalar is left at 1 (default).

Sr87_86_CorrRb: Interference- and mass-bias-corrected $^{87}Sr/^{86}Sr$ calculated by applying βRb to Rb but before final normalization of $^{87}Sr/^{86}Sr$ to a primary reference material. This will be the same as "87Sr_86_Corr" if "Rb Beta adjust" is not selected and the scalar is left at 1 (i.e., because βRb = βSr in this case).

Ho_Sr_ppm: (Only if "REE subtraction" is selected). Calculates the Ho signal (monitored on half-mass 82.5) relative to the total Sr signal in parts per million ($totalHo/totalSr*10^6$). Holmium is monoisotopic and is not used in any corrections, but can be used as a proxy for REE/Sr content of samples. This could also potentially be used (along with Er_Sr_ppm and Yb_Sr_ppm to calculate REE slopes to constrain Dy/Er).

Er_Sr_ppm: (Only if "REE subtraction" is selected). Calculates the total Er signal (monitored on half-mass 83.5 and calculated from canonical Er isotope abundances) relative to the total Sr signal in parts per million ($totalEr/totalSr*10^6$). This can be used as a proxy for REE/Sr content of samples. This could also potentially be used (along with Ho_Sr_ppm and Yb_Sr_ppm to calculate REE slopes to constrain Dy/Er).

Yb_Sr_ppm: (Only if "REE subtraction" is selected). Calculates the total Er signal (monitored on half-mass 86.5 and calculated from canonical Yb isotope abundances) relative to the total Sr signal in parts per million ($totalYb/totalSr*10^6$). This can be used as a proxy for REE/Sr content of samples. This could also potentially be used (along with Ho_Sr_ppm and Er_Sr_ppm to calculate REE slopes to constrain Dy/Er).

StdCorr_Sr87_86: Interference- and mass-bias-corrected $^{87}Sr/^{86}Sr$ calculated by applying βSr to Rb and normalized to $^{87}Sr/^{86}Sr$ of a primary reference material. This result is included so the $^{87}Sr/^{86}Sr$ calculated with and without the adjusted βRb can be compared.

Sr84_86_Corr: Interference- and mass-bias-corrected $^{84}Sr/^{86}Sr$. This stable Sr isotope ratio is sometimes used as an additional check to evaluate the effectiveness of the interference and mass-bias corrections. It is not normalized to a primary reference material, as this partly defeats the purpose of using it as an independent check.

Sr84_88_Corr: Interference- and mass-bias-corrected $^{84}Sr/^{88}Sr$. This stable Sr isotope ratio is sometimes used as an additional check to evaluate the effectiveness of the interference and mass-bias corrections. It is not normalized to a primary reference material, as this partly defeats the purpose of using it as an independent check.

Rb87_Sr86_Final: Final $^{87}Rb/^{86}Sr$ after interference, mass-bias, and elemental fractionation (if selected) corrections.

StdCorrRb_Sr87_86: Interference- and mass-bias-corrected $^{87}Sr/^{86}Sr$ calculated by applying βRb to Rb and normalized to $^{87}Sr/^{86}Sr$ of a primary reference material. This will be the same as "StdCorr_Sr87_86" if "Rb Beta adjust" is not selected and the scalar is left at 1 (i.e., because βRb = βSr in this case).

Sr87_86_AgeCorr: Age-corrected $^{87}Sr/^{86}Sr$. The result is always calculated with "Rb87_Sr86_Final", "StdCorrRb_Sr87_86", the ^{87}Rb decay constant of Villa et al. (2015), and the age of the sample in Ma entered by the user in the DRS settings. As of now, the calculation is applied to "StdCorrRb_Sr87_86" (i.e., before the CaPO correction, if selected), but this may be changed in the future.

CaPO_corrAmt: Model bias in $^{87}Sr/^{86}Sr$ according to the linear or exponential fit to the $^{87}Sr/^{86}Sr$ bias vs Sr signal (expressed as biased $^{87}Sr/^{86}Sr$ over "true" $^{87}Sr/^{86}Sr$). This is a function of total Sr signal intensity and is the correction factor that is applied the $^{87}Sr/^{86}Sr$ of the unknown (sample or secondary reference material) measurement.

CaPOCorr_Sr8786: Final $^{87}Sr/^{86}Sr$ after the CaPO correction. The CaPO correction is applied to StdCorrRb_Sr87_86" before age-correction.

References

Christensen, J. N., Halliday, A. N., Lee, D. C., & Hall, C. M. (1995). In situ Sr isotopic analysis by laser ablation. Earth and Planetary Science Letters, 136(1-2), 79-85.

Müller, W., & Anczkiewicz, R. (2016). Accuracy of laser-ablation (LA)-MC-ICPMS Sr isotope analysis of (bio) apatite–a problem reassessed. Journal of Analytical Atomic Spectrometry, 31(1), 259-269.

Nakamura, N. (1974). Determination of REE, Ba, Fe, Mg, Na and K in carbonaceous and ordinary chondrites. Geochimica et cosmochimica acta, 38(5), 757-775.

Villa, I. M., De Bièvre, P., Holden, N. E., & Renne, P. R. (2015). IUPAC-IUGS recommendation on the half life of 87Rb. Geochimica et Cosmochimica Acta, 164, 382-385.

Vroon, P. Z., Van Der Wagt, B., Koornneef, J. M., & Davies, G. R. (2008). Problems in obtaining precise and accurate Sr isotope analysis from geological materials using laser ablation MC-ICPMS. Analytical and Bioanalytical Chemistry, 390(2), 465-476.

Woodhead, J., Swearer, S., Hergt, J., & Maas, R. (2005). In situ Sr-isotope analysis of carbonates by LA-MC-ICP-MS: interference corrections, high spatial resolution and an example from otolith studies. Journal of Analytical Atomic Spectrometry, 20(1), 22-27.

Zhang, W., Hu, Z., Liu, Y., Wu, T., Deng, X., Guo, J., & Zhao, H. (2018). Improved in situ Sr isotopic analysis by a 257 nm femtosecond laser in combination with the addition of nitrogen for geological minerals. Chemical Geology, 479, 10-21.